Mobile robotic platforms for the acoustic tracking of deep-sea demersal fishery resources

I. Masmitja[1]*, J. Navarro[2], S. Gomariz[1], J. Aguzzi[2,3], B. Kieft[4], T. O'Reilly[4], K. Katija[4], P.J. Bouvet[5], C. Fannjiang[6], M. Vigo[2], P. Puig[2], A. Alcocer[7], G. Vallicrosa[8], N. Palomeras[8], M. Carreras[8], J. Del-Rio[1], J.B. Company[2]

[1] SARTI Research Group, Electronics Department, Universitat Politècnica de Catalunya, Barcelona, Spain.

[2] Institut de Ciències del Mar (ICM-CSIC), Barcelona, Spain.

[3] Stazione Zoologica Anton Dohrn, Naples, Italy.

[4] Research and Development, Monterey Bay Aquarium Research Institute, Moss Landing, U.S.A.

[5] L@BISEN, ISEN Brest Yncréa Ouest Brest, France.

[6] Department of Electrical Engineering and Computer Sciences, UC Berkeley, Berkeley, U.S.A.

[7] Department of mechanical, electronics and chemical engineering, Oslo Metropolitan University, Oslo, Norway.

[8] Computer Vision and Robotics Institute (VICOROB), Universitat de Girona, Girona, Spain.

* Corresponding author. Email: ivan.masmitja@upc.edu

Abstract

Knowing the displacement capacity and mobility patterns of industrially exploited (i.e. fished) marine resources is pivotal to establish effective conservation management strategies in a progressively anthropized ocean. To establish the sizes and adequate locations of marine protected areas within the framework of large international societal programs (e.g. European

This is an accepted, peer reviewed postprint-version of a journal article that has been published in Science robotics. DOI: https://doi.org/10.1126/scirobotics.abc3701

Community H2020, as part of the Blue Growth economic strategy), accurate behavioral information of deep-sea fished ecosystems is necessary but currently scarce and poorly accessible to high-frequency and prolonged data collection. A breakthrough in the autonomous capability of mobile platforms to deliver data on animal behavior beyond traditional fixed platform capabilities (e.g. cabled observatories or acoustic long-baseline systems) is overcoming these limitations. Here, we present useful example of that potential in relation to the implementation of autonomous underwater vehicles (AUVs) and remotely operated vehicles (ROVs) as an aid for acoustic long-baseline localization systems for autonomous tracking of Norway lobster (*Nephrops norvegicus*), one of the key living resources exploited in European waters. We reported the outcomes of that monitoring in combination with seafloor moored acoustic receivers to detect and track the movements of 33 tagged individuals at 400 m depth over more than three months. We identified best procedures to localize both the acoustic receivers and the tagged-lobsters, based on cutting-edge algorithms designed for off-the-self acoustic tags identification. These procedures represent an important step forward for prolonged, *in situ* monitoring of deep-sea benthic animal behavior at meter spatial scales.

Summary

Mobile robots with different degrees of platform operability are a key element to improve and extend the traditional acoustic tracking methods to study the spatiotemporal behavior of deep-sea fishery resources.

Introduction

The marine benthic realm is progressively becoming wired with cabled infrastructures in an attempt to transform strategic or protected areas (i.e. those of commercial or ecological value) into robotized laboratories with permanent monitoring functions (*1*, *2*). At the same time, other relevant oceanic-networks are being established worldwide, seeking to track the large-scale pelagic movements of species over large geographic areas and durations by animal-borne data-loggers (*3*–*6*). Data like these provide essential behavioral information for applying new cutting-edge conservation policies (*7*).

Large marine megafauna (e.g. cetaceans, dolphins, elasmobranchs or sea turtles), which rise to the sea surface habitually, allows the use of the data-loggers with global positioning system (GPS) and remote communication (e.g. Argos satellite network) to determine the duration and trajectories of those movements (*8*). However, never-surface emerging benthic and pelagic species cannot be tracked using such a methodology since electromagnetic waves suffer the drawbacks of high attenuation in seawater medium (*9*).

For those non-emerging benthic species, acoustic positioning methods from fixed platforms can be used alongside acoustic tags sensors deployed on animals (*10*), being tracked using long base-line (LBL) triangulation techniques (*11*). However, deploying benthic anchored receivers may increase operation complexity (e.g. in terms of spatial precision) and economic costs (*12*), with minimal flexibility (e.g. single location). Moreover, it is necessary to use specific tags in order to maintain synchronization between each receiver into the listening network, which may increase the complexity in data post-processing (*13*). While this technology has proven useful for behavioral tracking in shallow water scenarios (*14*), its performance has not yet been fully examined in the deep-sea. Only a few efforts have been conducted to follow populations movements over kilometer scales (*15*) with acoustic receivers mounted on moored of curtain or gate typologies (*16*).

A complementary strategy to the use of moored devices is to mount acoustic receivers on autonomous underwater vehicles (AUV), which is used as a virtual LBL, measuring the distance range with the target by acoustic modems (*17*, *18*). Differently from acoustic tags, these modems have bi-directional communications capabilities, and therefore, the time of flight (TOF) and slant range of an acoustic signal can be measured knowing the sound's velocity. Finally, triangulation localization techniques are applied to estimate the position of tagged-individuals with different algorithms (*19*). In addition, the bearing information estimated by ultra-short base-line (USBL) systems can also be used, which increases the overall speed response (*20*, *21*). Nevertheless, the investigations are again limited to large animals due to the size of electronic tags (*22*). Other authors use bearing-only techniques in order to avoid the use of acoustic modems and overcome the size limitations (*23*, *24*), where an AUV borne hydrophones' array is used to track acoustic tags. Unfortunately, a significant localization uncertainty is produced by the too-close positioning of hydrophones, which often requires larger separation that is not achievable on AUVs (*25*).

However, marine robots have in recent years been used for the tracking of marine species. For example, AUVs equipped with a single hydrophone were used to track fishes with different error ranges and procedures (e.g. SYNAPS and SPLWCA (*14*, *26*, *27*)). Some of the studies were conducted in combination with seafloor moored receivers, allowing records of the presence of tagged animals within the area of detection, but with high uncertainty in their position (*28*–*31*). Other authors used custom transponders attached to large marine species to increase the efficiency of vehicle tracking capabilities (*20*, *32*), but this approach is impractical for small marine species. Despite this interest, to our best knowledge, no previous study has addressed the tracking methodologies' performance by using static receivers and underwater vehicles, including testing its accuracy and capabilities in deep waters.

Here, we describe a new procedure for the multi tracking of one of the most important fishery resource in Europe, the Norway lobster (*Nephrops norvegicus* Linnaeus, 1758) (*33*), using a set of moored seabed receivers along with a remotely operated vehicle (ROV) and an AUV (Fig. 1). We developed a new area-only target tracking (AOTT) method to achieve active tracking of instrumented individuals, which only uses the detection pings of acoustic tags. Moreover, time difference of arrival (TDOA) algorithms have been adapted and tested to study their accuracy in variable operational scenarios. Specific objectives were: (i) TDOA algorithms performance comparison through Monte Carlo (MC) simulations; (ii) new AOTT algorithm capabilities presentation, where both simulations and field tests have been conducted; and (iii) the results of a 3-month campaign using static receivers (i.e. mooring lines with acoustic receivers) and underwater vehicles (an ROV and an AUV), where both TDOA and AOTT algorithms have been used. The tracking potential of this combined mobile and moored technology was tested in a deep-sea, no-take fishing zone under restoration, to show how a long-lasting acoustic-based deployment can provide new behavioral data that can inform the establishment and spatial extent of conservation areas.

Results

TDOA tracking algorithms performance

The performance of the different TDOA algorithms tested is presented in Fig. 2, where a set of MC simulations has been conducted. We used 4 receivers to localize a target on two-dimensional (2D) scenario, since the depth of the targets under study was known and constant as the species is benthic, with no swimming capability. These simulations are important to demonstrate the capabilities to track benthic tagged animals and to set the appropriate configuration (e.g. number of receivers, receivers' positions, or acoustic tag transmission period).

The Cramér-Rao bound (CRB) representation is presented in Fig. 2A, where 4 receivers with 200 m of baseline distance and a time error of 1 ms have been used (for other array configurations see Fig. S1). The area inside of the receivers' array showed the lowest expected measurement standard deviation error (< 1 m), whereas the error increased up to 7 m at 250 m off the receivers' array center.

To compare the algorithms' performance, a predefined target trajectory has been designed (Fig. 2B and Movie S1), according to which the target moves at 1 ms^{-1} among fourth receivers with a transmission period of 60 s. The root mean square error (RMSE) over the time is shown in Fig. 2C, where all the algorithms were iterated 100 times with a Gaussian error with 1 ms standard deviation (Fig. S2 shows the RMSE evolution with other errors). This result clearly showed that the error is lower inside the receivers' array, especially for the maximum likelihood (ML) estimation algorithm. That latter registered the greatest error. Due to numerical singularities around the receivers, the ML estimation failed to find the minimum of the cost function, and instead, it reached the local minimum nearby the receiver position. This problem was reduced by choosing a different initial estimation (i.e., closer to the real position), as explored with the weighted least squares ML (WLS-ML) algorithm, where the WLS method is used to initialize the ML estimation algorithm.

The algorithms' RMSE over the 100 MC iterations with different noise added in the time of arrival (TOA) measurements are presented in Fig. 2D. We simulated the algorithms' performance with noise standard deviation (σ) equal to 0.5, 1.0, and 1.5 ms. Moreover, additional tests with a Gaussian TOA error with $\sigma = 1.5$ ms plus 5% of outliers were simulated to observe the algorithms' behavior when facing strong multipath scenarios. These simulations showed that the particle filter (PF) had the best performance under different noise conditions, however, it had more difficulties to handle scenarios with outlier measurements, whereas the WLS excelled. In addition, the use of the WLS-ML combination slightly improved the algorithm's performance with different noise configurations. Nonetheless, this benefit was not observed in scenarios with outliers.

Finally, the average runtime required to compute one target position is shown in Fig. 2E, were the fastest algorithm was the WLS with 5 ms per iteration. In contrast, the PF required 977 ms, which means an increase of more than two orders of magnitude of the computational resources.

AOTT algorithm performance

A set of simulations were conducted to observe the optimal parameters for the AOTT algorithm (Fig. 3A) and the functions to weight the PF's particles (Fig. 3B). For example, the results showed a clear relationship between the tracker circumference radius (TCR) and the maximum transmission range (MTR), where the greatest ratio, $\Gamma_{\text{radius}} = TCR / MTR$, was equal to 0.8 (Fig. 3C). This means that the tracker had to conduct circumference maneuvers over the target estimation position with radius less than the MTR but closer to it. Nonetheless, is hard to known *a priori* the MTR achievable by an acoustic tag, which can be affected by different factors such as the sea state or the acoustic noise. Therefore, different *in situ* tests should be conducted to estimate its value. In our case, those tests pinpointed a maximum range less than 400 m with only a 20% of successful receptions (Fig. S3). In addition, the MTR is pivotal to spread the PF's particles, and therefore, different relationships between MTR and the maximum particles range (MPR) were studied, which allowed to identify the relation between the ratio $\Gamma_{\text{range}} = MPR / MTR$ and the AOTT's performance (see Fig. 3C). Moreover, the behavior of missing some of the tag's transmissions could also be observed, where the successful reception (SR) over the total transmissions (TT) ratio defined by $\Gamma_{\text{reception}} = SR / TT$ is presented. Finally, random particles were spread around the latest estimated target position (Compound resampling method), which helped to increase the particles diversity, and emphasized the latest time that the tag was detected, which yielded to an increase in tracking performance (see Fig. 3C).

The AOTT's performance can be observed on Fig. 3D (and Movie S2), where all the recommendations derived from the previous MC simulations presented above were used, which showed an error of ~ 100 m. After these simulations, a field test was conducted on June 27-28, 2018 (Fig. 3E) using the Monterey Bay Aquarium Research Institute (MBARI) coastal profile float (CPF) as a target (Fig. 3F) and a Wave Glider as a tracker (Fig. 3G) in Monterey Bay area, (CA, USA) (Fig. 3H). This test lasted more than 15 h, where the CPF conducted 3 immersions at 60 m depth.

Norway lobster tracking

The results of the four-step process to adjust the receiver clocks' drift and offset is shown in Fig. 4A–F, where a resolution greater than 2 ms was obtained. Moreover, a small number of outliers were detected during the post-processing (e.g. Fig. 4E), which had a random nature due to the homogeneous bathymetry of the experiment zone (i.e. a quasi-flat slope ground). In addition, the deployment position of the mooring lines using the oceanographic vessel's GPS, the ROV's USBL and the positions computed using the acoustic receivers are presented in Fig. 4G. Here, a great difference between the GPS's and ROV's positions could be observed, which pinpointed the necessity of the use of underwater vehicles to know final position of the receivers (Table 1).

After determining the receiver localizations and calibrating their clock offsets, the tagged Norway lobster positions could be tracked using the TDOA algorithms (see next section). The trajectory showed by each animal can be observed in Fig. 5A (and Movie S3), where the localization of the synchronization acoustic tags attached on the mooring lines, and the acoustic tags attached on the 33 individuals, are shown. After the canister release in the center of the receivers' array, the individuals show a dynamic dispersion and occupation of the monitored area. Furthermore, the accumulative distance of each individual was plotted in Fig. 5B, where we could appreciate how some animal went outside of the receivers' reception range, being therefore not detectable any more, from that moment on.

By the use of the two underwater robots (an ROV and an AUV), we could track the presence of some of those area-evading animals. The ROV conducted different lawn pattern movements on the southeast of the area, covering 10 km^2, and the AUV conducted a circumference path on the west (see Fig. 5C) with a radius equals to 150 m. During these tests, 4 tags were localized, and moreover, different images could be obtained, which will be used to study the seabed recovery in the protected areas (Fig. 5D and Movie S4).

Comparison between methods

The algorithms studied to track acoustic tags using the TDOA information could be compared together during the entire Norway lobster tracking experiment. Because the “true” position of the tagged lobsters was unknown, the synchronization tags attached on the mooring lines were used. In this case, the tags were not moving but static. Fig. 6A-6E show their estimated position and the error covariance matrix, which are represented as error bars in Fig. 6F (and summarized in Table S1). For example, the accuracy obtained to localize the lobster canister synchronization tag (i.e. base station (BS) D), which was placed in the receiver array center, was similar among all the algorithms (error <1 m). However, the PF had the poorest performance when it came to localize the synchronization tags attached on the mooring lines. This low performance was due to the nature of the PF’s particles distribution near the receivers in a TDOA topology (i.e. eccentricity of the hyperbola close to 1). Moreover, we found that both PF and WLS methods showed higher errors in positioning moorings Vemco acoustic receiver indicated as BS(D) and BS(E), which had different configuration (smaller dead weights and VR2AR-69k receivers). Taking into consideration the simulations conducted and the run-time required for each method, the WLS-ML offered the best reliability.

Finally, whereas the error of AOTT (order of tens of meters) is greater than the error that can be obtained with TDOA algorithms (order of few meters), the AOTT method overperforms these techniques due to the use of a single moving received on a mobile vehicle. This strategy, dramatically reduced infrastructure requirements.

Discussion

To the best of the authors' knowledge, this is the first study conducted to acoustically track tagged deep-sea benthic species, combining the information provided by underwater vehicles and anchored receivers, with meter spatial resolution. Here, the challenges of accurately positioning the receivers, adjusting the clocks' drift, and algorithms' performance have been analyzed, observing that are the primary cause of tracking success for an EU relevant fishery resource as the Norway lobster into a no-take zone. Thus, we set the basis and procedures which should be followed to obtain the best accuracy possible in similar operative deep-sea scenarios. In order to achieve such performance, the use of underwater mobile robotic platforms has been crucial, which can significantly boost traditional tracking methods (e.g. (*15*, *16*)), and extend target tracking beyond the limits of current LBL systems. In doing so, we have worked with two methods for target localization, which has been used in combination to extend their capabilities, (i) through static receivers anchored on the seabed and using TDOA algorithms, where a meter-resolution can be achieved, and (ii) using a single receiver installed on an underwater vehicle for dynamic tracking using the AOTT algorithm, which is capable to localize and track acoustic tags only by ping's detections.

Many efforts to study deep-sea species using acoustic target tracking systems has been conducted, and a complete survey of design settings, detection algorithms and used platforms are presented in Table 2. In this scenario, the strength of our contribution lies in the fact that we have faced the problem from a technological, operational and scientific point of view, covering different areas of study and sheds new light on the difficulties and solutions we encountered. We are confident that our results may improve knowledge about a comprehensive solution to track deep-sea species using both acoustic mooring receivers and underwater robotized platforms, which within the next years could be an important component in fishery resources management, and are destined to enable new scientific discoveries (*34*).

TDOA algorithms

This hyperbolic scheme is the method used when the acoustic target to be localized is not synchronized with the receivers or no bi-directional communications capability is available (*35*). In these cases, the slant range between target and receiver cannot be computed, and therefore, the triangulation methods for target localization based on range are not feasible. In a one-way communication scenario, the main problem to compute the TOF is to know the initial transmission time t_0. The TDOA was designed to avoid this inconvenient (*36*), where using two synchronized receivers, the unknown t_0 can be eliminated. In (*37*), the authors studied a method which estimated also the t_0, however this method has its limitations when the acoustic tag does not transmit in a specific and fixed period. Moreover, in (*35*) the authors studied analytically and through simulations different TDOA target localization algorithms, and found that it is not necessary to use the full set of TDOA measurements. In general, a set of L well-localized receivers are used, where there are $m = L(L-1)/2$ distinct TDOA measurements from all possible sensor pairs, which is known as the full TDOA set (*35*). With only a subset, one can achieve the same performance, but not when the target is outside of the center of the receivers' array (see Fig. S1). Moreover, we could observe that the WLS had the best performance, being also the fastest method. The target tracking experiments, in general, use a set of receivers anchored on the seabed (e.g. (*38*, *39*)). These receivers can operate for months continuously recording information of the tagged animals, and therefore, the number of measurements and consequently the number of computations required to track each animal can be significant. Thus, the runtime required is important in order to obtain the trustable tracking data.

AOTT algorithm

The area-based tracking method is used when the information to estimate the tag position is only the ping received by one receiver. Two sets of simulations with different reception ratios ($\Gamma_{reception}$) were conducted, using ratios equal to 100% and 60%. Before and after the target right turn (at 67 min from the beginning of the simulation), the error was $\sim 50\,\text{m}$ using the ideal reception ratio, and $\sim 100\,\text{m}$ using the 60% ratio. In this last situation, the AOTT had more problems to find and track the real target position, which lose the target position about $\sim 2\,\%$ of the iterations. Despite that, the tracker in general did not lose the target's position, and therefore, the great capabilities of the AOTT method were demonstrated in relation to previous efforts. For example, in (*23*) the authors used two hydrophones and bearing-only methods to track a tagged animal, resulting in critical consequences on vehicle's performance due to the payload's size, and drag effects of these hydrophones, with a reported error greater than 40 m. In order to increase the accuracy, the same authors presented a custom tag design (*32*), integrating an inertial measurement unit, which was used to adjust the velocity and attitude of the species during an offline post-processing. However, this approach augments considerably the tag's size, and therefore, is not suitable for smaller ones. The tag's size is also an important constrain in (*20*). In (*14*) the authors developed a method which uses the signal strength to infer the tag's position, nonetheless its performance and observability studies were not reported. Finally, in (*17*) a synthetic LBL is presented, where a constant, precise tag burst rate and a high resolution tag detection timestamp on the receiver are both necessary for estimating tag positions, which are not always possible.

From the AOTT's initial field test error, we could pinpoint three elements: (i) the algorithm was notably stable, where the target was mostly all the time localized; (ii) during the first CPF's immersion, the error was lower than 100 m, and then increased up to $\sim$ 100 m. If we compare this performance with the simulations conducted previously, and if we take into consideration that the Wave Glider's path was not optimal, the error's values were inside the expected boundaries; and

(iii) when the CPF was in the surface (i.e. at 5h) the error obtained was greater, probably due to poor tag reception.

Norway lobster tracking

We efficiently detected 33 tagged lobsters during several months with a high precision (i.e. less than 2 m) using the WLS-ML algorithm (see Table 1). Once the tagged animals were localized, their pattern of displacement could be inferred, e.g. using the joint estimation over multiple individuals method (*40*).

Nevertheless, the reception of the tags using the underwater vehicles was operationally complex. During the cruise, conducted after 5 months since the release of tagged-individuals, different dives were conducted with both the AUV and the ROV. Based on these dives, we were able to detect 4 Norway lobsters. In addition to the possibly that most of the tagged lobsters were lost or disappeared from the study area, the small number of detections could be caused by (i) acoustic interferences caused by the thrusters or the equipment installed on the vehicles (e.g. the USBL or the doppler velocity log), or (ii) due to lobster's diel burrow emergence patterns (*41*), since the acoustic signal could suffers strong attenuation while the individual is inside its burrow (*42*). For example, in (*31*) the authors used a Wave Glider to track Snow crabs (*Chionoecetes opilio*), which is powered by sea waves, and therefore, it does not use thrusters. Moreover, it does not use any acoustic positioning systems but GPS, as it stays permanently on the sea surface. Both aspects help to reduce the noise, and interferences with the tag's signal. This was also experimented during the AOTT field test, where the reception ratio was greater. Though, one of the main constrains for benthic deep-sea tag tracking is the maximum distance that an acoustic tag signal can be detected (e.g. less than 300 m for smaller devices), and therefore, the use of surface vehicles as Wave Gliders are not possible. One solution could be the use of an AUV with "silent" mode capabilities (i.e. dynamic buoyancy control) such as (*43*, *44*), or tethered the receiver at a sufficient distance.

Materials and Methods

Fieldwork experiments

Tracking procedures were conducted during 2019 in a no-take fishing zone, established at 380-400 m depth in the northwestern Mediterranean Sea (42º 00.8006' N and 03º 31.9723' E; Fig. 1E). During an oceanographic cruise on-board of the Research Vessel (R/V) García del Cid, on June 6, 2019, we deployed four mooring lines with Vemco receivers (Vemco, Canada): two equipped with VR2W-69k receivers and V7-69k synchronization tags; two equipped with VR2AR-69k acoustic release receivers. In the middle of these four mooring lines, we simultaneously released 33 Norway lobsters, each dorsally glued (i.e. cyanoacrylate) to a Vemco V7-69k tags, by using release canisters (an adaptation of (*42*)). All lobsters were captured in the study area with creels during the previous days before their release. The mooring lines with the receivers were recovered on September, 23, 2019 during a second oceanographic cruise on-board the R/V García del Cid.

In addition to the four mooring receivers, and also to detect the tagged-lobsters, during a third oceanographic cruise on-board the R/V Sarmiento de Gamboa in October 2019, we deployed two underwater vehicles in the same field site: an AUV (Girona 500 AUV, IQUA Robotics, Spain) and an ROV (Super Mohawk II, Forum Energy Technologies, Houston, TX, USA), both equipped with VR2W receivers.

Complementarily, some of these materials and procedures were tested on different preliminary operational calibration trials: (i) conducted at OBSEA observatory (www.obsea.es) deployed at 20 m depth and 4 km east off central Catalan coast, Barcelona (Mediterranean Sea), one of the three EMSO testing-sites (*45*, *46*), Fig. S4; and (ii) at Monterey Bay, California (USA), using the installations of MBARI.

Methodology

Four receivers created an acoustic LBL localization system, where each one was in self-recording mode and was not accessed in real time. The tags transmitted periodically an acoustic and individualized ping with a unidirectional communication protocol, which was recorded by the receivers. The tags were programmed to send this ping every 60 s (plus a random value up to 30 s to avoid multiple tags consistently overlap in time). Each tag transmits its own identifier using a pulse position modulation (PPM) with a carrier signal frequency of 69 kHz. The Vemco V7 tag has a typical working range of ~250 m, and therefore, the receivers' baseline was set to 200 m.

In addition, the V7 synchronization tags from Vemco were used to correct the receivers clock drift and to adjust the final receiver array position using a four-step process described below. These synchronization tags were attached on each mooring (1 m above the receivers) and to the lobster canister. During the experiment, both the ROV and the AUV positions were known using the R/V's USBL. Also, the AUV had its own dead reckoning system for autonomous navigation. The final position of the receivers could be computed using the information provided by the ROV's USBL, which was more exact than the deployment position obtained on surface with the GPS of the R/V due to the drift during the 400 m dive. The ROV was piloted above the moorings and its position was used as a "true" position of two of them. Then, knowing the TOF among the other lines and the lobster canister through the synchronization tags and the receivers, their relative positions could be determined by simple trigonometry functions and rotation matrices.

TDOA algorithms

Target localization using TDOA is a well-known problem which has been addressed on both terrestrial and underwater environments during the last decades. The TDOA has been usually used when no synchronization between transmitters and receivers can be enforced, and even more, if transmitters ping-time is irregular (e.g. using Vemco devices). In both cases, the TOF cannot be measured or estimated, and consequently, the TDOA between different pair of receivers is used.

In general, TDOA algorithms can be divided in two groups, the ML and least-squares (LS) methods (*47*). Using $n+1$ receivers (where $n \in \{2,3\}$ is the space dimensionality of the problem) a set of hyperbolic equations can be obtained to find the coordinates of the target. The TDOA measurement between two receivers $\mathbf{b} \in \mathbb{R}^n$ and the target at position $\mathbf{q} \in \mathbb{R}^n$ can be written as

$$\begin{aligned}\mu^{ij}(\mathbf{x}) &= (t_0 + \frac{1}{c}\|\mathbf{q}-\mathbf{b}_i\|) - (t_0 + \frac{1}{c}\|\mathbf{q}-\mathbf{b}_j\|) + w \\ &= \frac{1}{c}(\|\mathbf{q}-\mathbf{b}_i\| - \|\mathbf{q}-\mathbf{b}_j\|) + w\end{aligned}, \quad (1)$$

where $i, j \in \{0, \ldots, m\}$ and $i \neq j$, c is the sound velocity in water, and t_0 is the target transmission time. Assuming a zero-mean white Gaussian error noise distribution of the TDOA measurements, i.e. $w \sim \mathcal{N}(0,\sigma^2)$ with variance σ^2, the unknown parameter $\mathbf{q} \in \mathbb{R}^n$ can be estimated using the ML estimation method. In this case, the density function for each $\mu^{ij}(\mathbf{q})$ is given by

$$f(\mathbf{q}) = \frac{1}{\sqrt{2\pi\sigma^2}} \exp\left(-\frac{\left(\bar{\mu}^{ij} - \mu^{ij}(\mathbf{q})\right)^2}{2\sigma^2}\right), \quad (2)$$

where $\bar{\mu}$ represents the measured TDOA. Given a vector of observations $\bar{\boldsymbol{\mu}} \in \mathbb{R}^m$ the function $\mathcal{L}: \mathbb{R}^n \to [0,1] \subset \mathbb{R}$ which for any target position $\mathbf{q} \in \mathbb{R}^n$ yields the probability $p(\bar{\boldsymbol{\mu}} \mid \mathbf{q})$, is referred to as the *likelihood function*, given by

$$\begin{aligned}
\mathcal{L}(\mathbf{q}) &:= p(\bar{\boldsymbol{\mu}} \mid \mathbf{q}) = \prod_{k=1}^{m} \frac{1}{\sqrt{2\pi\sigma^2}} \exp\left(-\frac{\left(\bar{\mu}^k - \mu^k(\mathbf{q})\right)^2}{2\sigma^2} \right) \\
&= \left(\frac{1}{\sqrt{2\pi\sigma^2}} \right)^m \exp - \frac{1}{2\sigma^2} \sum_{k=1}^{m} \left(\bar{\mu}^k - \mu^k(\mathbf{q})\right)^2 \\
&= \frac{1}{(2\pi)^{\frac{m}{2}} \, |\mathbf{R}|^{\frac{1}{2}}} \exp\left(-\frac{1}{2} \| \bar{\boldsymbol{\mu}} - \boldsymbol{\mu}(\mathbf{q}) \|_{\mathbf{R}}^2 \right)
\end{aligned}, \qquad (3)$$

where $\| \mathbf{a} \|_{\mathbf{M}}^2 \triangleq \mathbf{a}^T \mathbf{M}^{-1} \mathbf{a}$, and $\mathbf{R}$ is the covariance matrix, and $\mathbf{I}_m$ is the identity matrix of dimension $m \times m$. The ML estimator is defined as

$$\hat{\mathbf{q}} = \underset{\mathbf{q} \in \mathbb{R}^n}{\arg\max}\, \mathcal{L}(\mathbf{q}). \qquad (4)$$

A common practice in ML estimation is to work with the *log-likelihood function*. Since the logarithm is a strictly increasing function, and $\mathcal{L}(\mathbf{q})$ is strictly positive, maximizing the *likelihood* and the *log-likelihood* are equivalent. Neglecting constant terms, the ML estimator can be found by solving the optimization problem

$$\hat{\mathbf{q}} = \underset{\mathbf{q} \in \mathbb{R}^n}{\arg\min}\; f(\mathbf{q}), \qquad (5)$$

where $f: \mathbb{R}^n \to \mathbb{R}$ is given by the following cost function

$$f(\mathbf{q}) := \frac{1}{2} \| \bar{\boldsymbol{\mu}} - \boldsymbol{\mu}(\mathbf{q}) \|_{\mathbf{R}^2}^2 = \frac{1}{2} \left(\bar{\boldsymbol{\mu}} - \boldsymbol{\mu}(\mathbf{q}) \right)^T \mathbf{R}^{-1} \left(\bar{\boldsymbol{\mu}} - \boldsymbol{\mu}(\mathbf{q}) \right). \qquad (6)$$

In general, there is no closed form solution to the previous optimization problem. The cost function is relatively complex, nonlinear and even not differentiable at some points because of the square roots that defines the TDOA measurements.

A standard approach for its optimization is to employ Newton-Raphson iterative minimization (*48*). In order to implement gradient and Newton descent algorithms to minimize the cost function it is necessary to have expressions for its gradient $\nabla f(\mathbf{q})$ and Hessian $\nabla^2 f(\mathbf{q})$, which are the vector of its first partial derivatives and matrix of its second partial derivatives respectively. This can be done resorting to Matrix Differential Calculus, see (*11*, *49*) and the references therein.

Nonlinear estimation problems are also often addressed using linearized estimators, e.g., the extended Kalman filter (EKF) (*50*). However, linearization-based filtering approach marginalize all but the current state and is hence unable to refine past linearization points. In contrast, a batch maximum a posteriori (MAP) estimator computes the estimates for the states at all-time steps using all available measurements (*51*). The difference between MAP and ML estimation lies in the assumption of an appropriate prior distribution of the parameters to be estimated (*52*). The MAP estimator utilizes all available information to estimate the entire target's trajectory which is represented by stacking all states in the time interval $[0, \mathrm{k}]$ as

$$\mathbf{x}_{0:\mathrm{k}} = \begin{bmatrix} \mathbf{x}_0^T & \mathbf{x}_1^T & \dots & \mathbf{x}_\mathrm{k}^T \end{bmatrix}^T, \quad (7)$$

where $\mathbf{x}_k = \begin{bmatrix} x_{qk} & \dot{x}_{qk} & y_{qk} & \dot{y}_{qk} \end{bmatrix}^T \in \mathbb{R}^{2n}$ is the target's position and all the higher order time derivatives (i.e. velocity or acceleration). In addition, a motion model is used, which typically consider that the target moves randomly but assume that a stochastic kinematic model describing its motion (e.g., constant velocity) is known. Thus, the discrete-time state propagation equation is generally given by

$$\mathbf{x}_k = \Phi_{k-1}\mathbf{x}_{k-1} + \mathbf{w}_{k-1}, \quad (8)$$

where $\mathbf{w}_{k-1}$ is zero-mean white Gaussian noise with covariance $\mathbf{Q}$, and the state transmission matrix, Φ_{k-1}, is given by

$$\Phi_{k-1} = \begin{bmatrix} 1 & \Delta t & 0 & 0 \\ 0 & 1 & 0 & 0 \\ 0 & 0 & 1 & \Delta t \\ 0 & 0 & 0 & 1 \end{bmatrix}. \tag{9}$$

Then, the MAP estimator seeks to determine the entire state-space trajectory that maximizes the following posterior probability density function

$$\begin{aligned} & p(\bar{\boldsymbol{\mu}}_{1:k} \mid \mathbf{x}_{0:k}) \propto \\ & \frac{1}{(2\pi)^{n} \mid \mathbf{P}_{0|0} \mid^{\frac{1}{2}}} \exp\left(-\frac{1}{2} \| \mathbf{x}_{0} - \hat{\mathbf{x}}_{0|0} \|^{2}_{\mathbf{P}_{0|0}} \right) \\ & \times \prod_{k=1}^{\mathrm{k}} \frac{1}{(2\pi)^{n} \mid \mathbf{Q}^{'} \mid^{\frac{1}{2}}} \exp\left(-\frac{1}{2} \| \mathbf{x}_{k} - \mathbf{\Phi}_{k-1} \mathbf{x}_{k-1} \|^{2}_{\mathbf{Q}^{'}} \right), \\ & \times \prod_{k=1}^{\mathrm{k}} \frac{1}{(2\pi)^{\frac{m}{2}} \mid \mathbf{R}_{k} \mid^{\frac{1}{2}}} \exp\left(-\frac{1}{2} \| \bar{\boldsymbol{\mu}}_{k} - \boldsymbol{\mu}(\mathbf{q}_{k}) \|^{2}_{\mathbf{R}} \right) \end{aligned} \tag{10}$$

where a prior distribution equal to $p(\mathbf{x}_0) = \mathcal{N}(\hat{\mathbf{x}}_{0|0}, \mathbf{P}_{0|0})$ has been used, and $\bar{\boldsymbol{\mu}}_{1:k}$ denotes all the measurements in the time interval $[1, \mathrm{k}]$. Using the same procedure as in eq. (3), the cost function is given by

$$\begin{aligned} & f(\mathbf{x}_{0:\mathrm{k}}) := \frac{1}{2} \| \mathbf{x}_{0} - \hat{\mathbf{x}}_{0|0} \|^{2}_{\mathbf{P}_{0|0}} \\ & + \sum_{k=1}^{\mathrm{k}} \frac{1}{2} \| \mathbf{x}_{k} - \mathbf{\Phi}_{k-1} \mathbf{x}_{k-1} \|^{2}_{\mathbf{Q}^{'}} \quad . \\ & + \sum_{k=1}^{\mathrm{k}} \frac{1}{2} \| \bar{\boldsymbol{\mu}}_{k} - \boldsymbol{\mu}(\mathbf{q}_{k}) \|^{2}_{\mathbf{R}} \end{aligned} \tag{11}$$

And finally, the solution can also be computed employing Newton-Raphson iterative minimization methods, see (*51*) and references therein. However, this solution, heavily depends on the quality of the initial estimate, especially if multi-modal probability density functions are involved (i.e., the solution may lie on local minimum instead of the true target position).

To estimate multi-modal distributions, one of the most used methods is the PF (*53*, *54*). The PF solves in a non-parametric way the probability distribution problem using a set of particles, $\mathbf{x} \in \mathbb{R}^{2n}$, which are spread on the area in order to represent the true distribution. Each particle represents a hypothesis of the target state. The particles are weighted and normalized based on their measurement likelihood, and resampled accordingly (*55*, *56*).

Another method to solve the likelihood function eq. (3) is using a closed-form LS solution. A wide used closed-form method was developed by Chan and Ho (*36*). They give an alternative solution for hyperbolic position fix by using an approximation of the ML estimation when the TDOA estimation errors are small. The original set of TDOA equations are transformed into another set $\mathbf{x} = \begin{bmatrix} \mathbf{q}^T & r_0 \end{bmatrix}^T \in \mathbb{R}^{n+1}$, which are linear in source position coordinates $\mathbf{q}$, and adding an extra variable r_0, which is the range between the target and the reference sensor. Then, the algorithm uses a two-step WLS method to estimate the target position, which is given by

$$\mathbf{x} = \left(\mathbf{G}_a^T \boldsymbol{\Psi}^{-1} \mathbf{G}_a\right)^{-1} \mathbf{G}_a^T \boldsymbol{\Psi}^{-1} \mathbf{h}, \qquad (12)$$

Where

$$\mathbf{G}_a = \begin{bmatrix} \mathbf{b}_{10}^T & r_{10} \\ \mathbf{b}_{20}^T & r_{10} \\ \vdots & \vdots \\ \mathbf{b}_{L0}^T & r_{10} \end{bmatrix}, \mathbf{h} = \frac{1}{2} \begin{bmatrix} \|\mathbf{b}_1\|^2 - \|\mathbf{b}_0\|^2 - {r_{10}}^2 \\ \|\mathbf{b}_1\|^2 - \|\mathbf{b}_0\|^2 - {r_{10}}^2 \\ \vdots \\ \|\mathbf{b}_1\|^2 - \|\mathbf{b}_0\|^2 - {r_{10}}^2 \end{bmatrix}, \boldsymbol{\Psi} = c^2 \mathbf{B}_a \mathbf{R} \mathbf{B}_a, \qquad (13)$$

and $\mathbf{B}_a = \|\mathbf{q} - \mathbf{b}_0\| \mathbf{I}_m$.

Further, different authors have improved this technique, for example, in (*57*) the WLS includes a vertical plane constraint and a cone tangent plane constraint. These two constraints are derived from the initial value and updated again after each iteration.

Finally, in (*37*) the authors developed the yet another positioning solver (YAPS) method, where they used the TOA instead of the TDOA to estimate the target position. Because of that, they had to also estimate the target transmission time t_k. The modelling follows the state space paradigm, which uses the process and observation models as in MAP estimation method. They used a stochastic processes to describe the state propagation as a random walk with different degrees of standard deviation for both transmission time $t_k - t_{k-1} \sim \mathcal{N}(t_{k-1} - t_{k-2}, \sigma_{bi}^2)$ and target position $\mathbf{q}_k \sim \mathcal{N}(\mathbf{q}_{k-1}, 2D_{xy}\Delta t^{0.5})$, where D_{xy} is the diffusivity. The YAPS method is coded as a C++ file, which evaluates the joint density through the template model builder (TMB) framework. That latter uses the Laplace approximation to find the unobserved random variables (e.g. x, y, and t), and the parameters (e.g. D_{xy}) that can be estimated using the ML principle and built-in optimizer in R. Therefore, this model analysis follows a standard ML analysis of non-linear mixed-effects model, suing the TMB as the computational tool to automatize the process with R software.

Here, all these algorithms have been compared with the CRB (*58*), which sets the lowest bound on the performance of unbiased estimators that use observations according to a certain probability density function. This bound is one of the most widely used (*59–61*), which for a TDOA target localization problem is given by

$$\mathrm{Cov}\,\{\hat{\mathbf{q}}\} \succeq \mathbf{I}(\mathbf{q})^{-1}, \tag{14}$$

where $\mathbf{I}$ denotes the Fisher Information Matrix (FIM) defined as

$$\mathbf{I}(\mathbf{q}) = \nabla f(\mathbf{q})^T \mathbf{R}^{-1} \nabla f(\mathbf{q}), \tag{15}$$

where $\nabla f(\mathbf{q})$ is the gradient of the *log likelihood* function with respect to the unknown parameters, which has been used to compute the target position using the ML estimation. Taking the trace of $\mathbf{I}$ we obtain a new inequality, which sets a fundamental lower bound on the mean-square error of any unbiased estimator, given by

$$\operatorname{var}\left\{\hat{\mathbf{q}}\right\} = \mathrm{E}\left\{\|\hat{\mathbf{q}}(\bar{\mu}) - \mathbf{q}\|^2\right\} \geq \operatorname{tr}\left(\mathbf{I}(\mathbf{q})^{-1}\right) \tag{16}$$

TDOA Simulations

Different simulations have been conducted in order to characterize the TDOA target localization algorithms explained above under different parameters and scenarios. These simulations have been carried out using the MC simulation method. For all the simulations, the RMSE has been computed using the median, and the 5th and 95th percentile, over 100 iterations, where different TDOA Gaussian noise has been added using $\sigma = 0.5$ ms, $\sigma = 1$ ms, and $\sigma = 1.5$ ms. The parameters of the scenario simulated used were: (i) tag transmission delay = 120 s, (ii) target velocity = 0.2 m/s, and (iii) number of particles (for the PF algorithm) = 6000 particles. Algorithms' run-time has been obtained using a Processor Intel® Core™ i7-4760HQ CPU @ 2.10 GHz with 8 GB of RAM memory.

Receiver clock drift adjustment and localization

Four receivers have been used in this study, where each one has an internal clock which is not synchronized periodically. Consequently, during the campaign they suffered from drift and misalignment. This behavior introduces an error which must be fixed for twofold: (i) to be able to associate independent receptions at separate receivers, corresponding to the same target and emission time, and (ii) to compute the TDOA accurately. The TDOA between two receivers (considering their clocks' drift) can be modelled as

$$\mu_k^{ij}(\mathbf{q}) = \frac{1}{c}\left(\|\mathbf{q}_k - \mathbf{b}_i\| - \|\mathbf{q}_k - \mathbf{b}_j\|\right) + \left(C_{ik} - C_{jk}\right), \tag{17}$$

where C_{ik} is the clock's misalignment of receiver i at time step k. Considering static receivers and a static acoustic tag $\mathbf{q}_0$ (typically localized in the center of the receivers' array), the measurement $\mu_k^{ij}(\mathbf{q}_0)$ should be constant. However, due to the differences in the clocks' drift $C_{ij} = C_{ik|_{\mathbf{q}_0}} - C_{jk|_{\mathbf{q}_0}}$ this is not true, which would result in target localization errors. Therefore, here we developed a procedure to adjust the drift using a four-step process: (i) using the initial points and a linear regression, (ii) using a polynomial regression with all the points, (iii) using different polynomial regression functions at different segments of data, and (iv) using the distance difference to correct the offset.

The first step was used to adjust the main drift, which is necessary to associate independent receptions at separate receivers. If the clock's drift is greater than the acoustic tag transmission interval time, it is not possible to associate the receptions of an acoustic tag transmission at different independent receivers (in long field studies, i.e. more than one month, the drift can reach more than 30 seconds). Thus, only the initial points can be used. Then, the different receptions can be associated and a polynomial fitted curve can be used to eliminate the main clocks' drift for the entire data. In addition, the whole data was segmented into small portions (e.g., by weeks), and a second polynomial fitted curve was used for a fine tune. With this procedure, the drift was adjusted (i.e. the slope of the C_{ij}, aka C_{ij}^{slope}). Nonetheless, a final step to adjust the clocks' offset was still necessary. We know that the distance between the receiver pair ij have to be equal to the distance between the receiver pair ji, and therefore, an offset equal to $C_{ij}^{offset} = \left(d_{ij} - d_{ji}\right)/2$ can be added. Thus, each clock's receiver adjustment is given by

$$Clk_{i,n} = \sum_{r=0}^{N} C_{ij,(N-r)}^{slope} Clk_{i,n}{}^{r} + C_{ij}^{offset}, \tag{18}$$

where $Clk_{i,n}$ is the timestamp value n of receiver i, and N is the polynomial degree of the fitting curve.

Once the internal clock drift was adjusted, the position of each receiver $\mathbf{b}_i$ could be computed. First, the distance among each receiver d_{ij} were calculated using the TOF, which was known due to the fact that each receiver had also a synchronization acoustic tag attached on the mooring line, and therefore, the t_0 was known. Then, the $\mathbf{b}_i$ positions were computed using these distances and trigonometry. Finally, the positions were adjusted using a rotation matrix and a translation matrix to obtain the final position referenced to the geographic coordinates system, where the mooring anchors' positions found by the ROV were used.

AOTT algorithm

The AOTT method uses a single moving receiver, and therefore, no TDOA information is present. In its place, the tag's position is estimated by using the ping detection/no-detection information provided by a receiver. However, the detection of a tag's transmission is complex due to acoustic noise form platforms' thrusters, multipath, or distance between the tag and the receiver. Consequently, the AOTT algorithm attributes such as the reception ratio or maximum transmission range have been studied through simulations and field tests before the Norway lobsters' field survey.

Given the acoustic receiver and transmitter tag used for this work, the only information that can be determined is the presence or absence of acoustic tag transmissions in the area of the receiver, without information about the tag's direction or range of detection. The AOTT method infers the target position by taking the area determined by the maximum reception range as the only filter input (*62*). Two types of areas can be defined: one where the tag is detected, and one where the tag is not detected. The estimation of the target's localization can then be computed by overlapping all of these areas, where the zone with a main coincidence is where the target should be, thereby representing its probability distribution.

The AOTT was implemented by using a PF algorithm, where a set of particles $\mathbf{x} \in \mathbb{R}^{2n}$ are randomly spread in the area, and then, each particle is moved accordingly to a motion model eq. (8), and each particle's weight is updated for each new detection (or no-detection) until all of them converge into the target position estimation. Therefore, the probability distribution function can be derived using the Bayes' rule (*63*) with the recursion of the prediction step

$$p(\mathbf{x}_k \mid \mathbf{z}_{:k-1}) = \sum_{\mathbf{x}_k - 1} \underbrace{p(\mathbf{x}_k \mid \mathbf{x}_{k-1})}_{\text{Motion model}} \underbrace{p(\mathbf{x}_{k-1} \mid \mathbf{z}_{:k-1})}_{\text{Particles}}, \tag{19}$$

and the update state

$$p(\mathbf{x}_k \mid \mathbf{z}_{:k}) \propto \underbrace{p(\mathbf{z}_k \mid \mathbf{x}_k)}_{\text{Importance weights}} \underbrace{p(\mathbf{x}_k \mid \mathbf{z}_{:k-1})}_{\text{Particles}}, \tag{20}$$

where $\mathbf{z} \in \mathbb{R}^m$ are a set of measurements.

The main difference between the range-only (*19*) and area-only target tracking algorithm based on PF is how the particles are weighted. In a range-only method, the likelihood ratio based on the measurement probability function is described as

$$W_k^n = \frac{1}{\sqrt{2\pi\sigma_w^2}} \exp\left(-\frac{\left(\bar{z}_k - z(\mathbf{x}_k^n)\right)^2}{2\sigma_w^2} \right), \tag{21}$$

in this case, the index $n \in \{0, \ldots, N\}$ indicates the particle number up to N.

Whereas in the area-only method, the measurement probability function is based on the distance that each particle has between each other and the observer, where the particles which are inside the area defined by the maximum range that an acoustic tag can be detected will be more weighted than the particles which are outside of this area. Moreover, if an acoustic tag detection is missed, the particles inside the area will be less weighted than the particles which are outside.

This behavior can be represented using the cumulative distribution function (CDF) (*64*) and its complementary survival function (SF) (known also as Q-function (*65*)), which are given by

$$W_k^n = \begin{cases} \dfrac{1}{\sqrt{2\pi\sigma_w^2}} \displaystyle\int_{-\infty}^{r} \exp\left(-\dfrac{(\mathrm{x} - \mu)^2}{2\sigma_w^2}\right) d\mathrm{x} & \text{if } z_m = 1 \\ 1 - \dfrac{1}{\sqrt{2\pi\sigma_w^2}} \displaystyle\int_{-\infty}^{r} \exp\left(-\dfrac{(\mathrm{x} - \mu)^2}{2\sigma_w^2}\right) d\mathrm{x} & \text{if } z_m = 0 \end{cases}, \qquad (22)$$

where r is the distance between each particle and the observer, μ is the maximum range that an acoustic tag can be detected, and σ_w^2 is the variance, which is used to modify the slope of the function. In addition, the resampling method used in PF has also an important impact on its performance. As was pinpointed in (*66*), a Compound resampling method can improve the target accuracy. The main idea of the Compound method is to spread a certain number of particles randomly. In this case, the random particles are spread around the latest estimated target position, which helps to increase the particles diversity, and emphasize the latest time that the tag was detected.

AOTT simulations

The idea of observability in target tracking using a single vehicle is of primary importance (*67*–*69*), which is related to the local weak observability properties for a specific non-linear system. The observability problem is concerned with determining conditions under which a knowledge of the input-output data uniquely determines the state of the system (*70*), e.g., the optimal path that should be conducted by the vehicle to maximize the accuracy of the estimated target position (*71*–*73*). These studies pinpointed two basic rules to follow: (i) all measurements must be performed uniformly distributed on a circumference centered over the target, and (ii) the circumference's radius must be greater than the target depth and in some cases as large as possible. Using these two ideas, we conducted different simulations to characterize the AOTT algorithm under different parameters and scenarios, which were used to optimize the algorithm's parameters and tracker's path. These simulations had been carried out using the MC simulation method. For all the simulations, the mean and the average result after 30 iterations are presented. The other parameters, which are not involved in the current simulation, had been considered ideal. Two different scenarios had been developed for each case: (i) localizing a static target, and (ii) tracking a moving target with a velocity equal to 0.2 m/s. The weight's distribution used in the area-only method was computed using a $\sigma_W = 4.5\,\mathrm{m}$ for the SF, and a $\sigma_W = 9\,\mathrm{m}$ for the CDF functions, which were detection and no-detection scenarios respectively.

A second set of simulations was carried out to observe the AOTT's performance using all the results derived from the previous section. In this case, the target was moving at 0.2 m/s and performed a 90º right turn after 67 min, the rest of the parameters were: (i) tag transmission delay = 60 s, (ii) maximum tag transmission range = 250 m, (iii) tracker radius = 200 m, (iv) tracker velocity = 1 m/s, (v) number of particles = 10000, (vi) resampling method = Compound with ratio 1.5%, (vii) maximum particles range = 300 m, and (viii) number of iterations = 50.

AOTT test

Experimental field testing were conducted on June 27-28, 2018 using a Wave Glider (Liquid Robotics, USA) as a tracker and the MBARI's CPF (*74*) as a target. The Wave Glider was equipped with a Vemco receiver (VR2C-69kHz, Vemco, Canada), and two Vemco acoustic tags (V7P-69k, Vemco, Canada) were installed to the CPF. Additionally, the CPF was equipped with a Benthos acoustic modem (ATM-900, Teledyne Marine – Benthos, USA) and the Wave Glider with a Benthos DAT (direction acoustic transponder) modem (DAT, Teledyne Marine – Benthos, USA), which is a type of USBL. This test lasted more than 15 h, where the CPF conducted 3 immersions at $\sim 60\,\mathrm{m}$ depth. During the tests, the Wave Glider carried out different circumferences around the area (manually piloted) which were used in twofold purposes: (i) to perform an acoustic tag detection ratio versus range test, finding the maximum range where the tags could be detected; and (ii) to compare the accuracy of the USBL, the range-only target tracking (ROTT), and the AOTT methods.

References

1. R. Danovaro, J. Aguzzi, E. Fanelli, D. Billett, K. Gjerde, A. Jamieson, E. Ramirez-Llodra, C. R. Smith, P. V. R. Snelgrove, L. Thomsen, C. L. Van Dover, An ecosystem-based deep-ocean strategy. *Science (80-.).* **355**, 452–454 (2017).
2. J. Aguzzi, D. Chatzievangelou, S. Marini, E. Fanelli, R. Danovaro, S. Flögel, N. Lebris, F. Juanes, F. C. De Leo, J. Del Rio, L. Thomsen, C. Costa, G. Riccobene, C. Tamburini, D. Lefevre, C. Gojak, P. M. Poulain, P. Favali, A. Griffa, A. Purser, D. Cline, D. Edgington, J. Navarro, S. Stefanni, S. D'Hondt, I. G. Priede, R. Rountree, J. B. Company, New High-Tech Flexible Networks for the Monitoring of Deep-Sea Ecosystems. *Environ. Sci. Technol.* **53**, 6616–6631 (2019).
3. B. A. Block, I. D. Jonsen, S. J. Jorgensen, A. J. Winship, S. A. Shaffer, S. J. Bograd, E. L. Hazen, D. G. Foley, G. A. Breed, A.-L. Harrison, J. E. Ganong, A. Swithenbank, M. Castleton, H. Dewar, B. R. Mate, G. L. Shillinger, K. M. Schaefer, S. R. Benson, M. J. Weise, R. W. Henry, D. P. Costa, Tracking apex marine predator movements in a dynamic ocean. *Nature*. **475**, 86–90 (2011).
4. N. E. Hussey, S. T. Kessel, K. Aarestrup, S. J. Cooke, P. D. Cowley, A. T. Fisk, R. G. Harcourt, K. N. Holland, S. J. Iverson, J. F. Kocik, J. E. Mills Flemming, F. G. Whoriskey, Aquatic animal telemetry: A panoramic window into the underwater world. *Science (80-.).* **348**, 1255642–1255642 (2015).
5. J. McGowan, M. Beger, R. L. Lewison, R. Harcourt, H. Campbell, M. Priest, R. G. Dwyer, H. Y. Lin, P. Lentini, C. Dudgeon, C. McMahon, M. Watts, H. P. Possingham, Integrating research using animal-borne telemetry with the needs of conservation management. *J. Appl. Ecol.* **54**, 423–429 (2017).
6. R. Harcourt, A. M. M. Sequeira, X. Zhang, F. Roquet, K. Komatsu, M. Heupel, C. McMahon, F. Whoriskey, M. Meekan, G. Carroll, S. Brodie, C. Simpfendorfer, M. Hindell, I. Jonsen, D. P. Costa, B. Block, M. Muelbert, B. Woodward, M. Weise, K. Aarestrup, M. Biuw, L. Boehme, S. J. Bograd, D. Cazau, J. B. Charrassin, S. J. Cooke, P. Cowley, P. J. N. de Bruyn, T. Jeanniard du Dot, C. Duarte, V. M. Eguíluz, L. C. Ferreira, J. Fernández-Gracia, K. Goetz, Y. Goto, C. Guinet, M. Hammill, G. C. Hays, E. L. Hazen, L. A. Hückstädt, C. Huveneers, S. Iverson, S. A. Jaaman, K. Kittiwattanawong, K. M. Kovacs, C. Lydersen, T. Moltmann, M. Naruoka, L. Phillips, B. Picard, N. Queiroz, G. Reverdin, K. Sato, D. W. Sims, E. B. Thorstad, M. Thums, A. M. Treasure, A. W. Trites, G. D. Williams, Y. Yonehara, M. A. Fedak, Animal-borne telemetry: An integral component of the ocean observing toolkit. *Front. Mar. Sci.* **6** (2019), doi:10.3389/fmars.2019.00326.
7. G. C. Hays, H. Bailey, S. J. Bograd, W. D. Bowen, C. Campagna, R. H. Carmichael, P. Casale, A. Chiaradia, D. P. Costa, E. Cuevas, P. J. Nico de Bruyn, M. P. Dias, C. M. Duarte, D. C. Dunn, P. H. Dutton, N. Esteban, A. Friedlaender, K. T. Goetz, B. J. Godley, P. N. Halpin, M. Hamann, N. Hammerschlag, R. Harcourt, A. L. Harrison, E. L. Hazen, M. R. Heupel, E. Hoyt, N. E. Humphries, C. Y. Kot, J. S. E. Lea, H. Marsh, S. M. Maxwell, C. R. McMahon, G. Notarbartolo di Sciara, D. M. Palacios, R. A. Phillips, D. Righton, G. Schofield, J. A. Seminoff, C. A. Simpfendorfer, D. W. Sims, A. Takahashi, M. J. Tetley, M. Thums, P. N. Trathan, S. Villegas-Amtmann, R. S. Wells, S. D. Whiting, N. E.

Wildermann, A. M. M. Sequeira, Translating Marine Animal Tracking Data into Conservation Policy and Management. *Trends Ecol. Evol.* **34**, 459–473 (2019).
8. R. Kays, M. C. Crofoot, W. Jetz, M. Wikelski, Terrestrial animal tracking as an eye on life and planet. *Science (80-.).* **348**, aaa2478 (2015).
9. W. S. Burdic, *Underwater Acoustic System Analysis, Second Edition* (Peninsula Publishing, Second edi., 2002).
10. L. Paull, S. Saeedi, M. Seto, H. Li, AUV navigation and localization: A review. *IEEE J. Ocean. Eng.* **39**, 131–149 (2014).
11. A. Alcocer, Positioning and navigation systems for robotic underwater vehicles, PhD thesis, Universidade Técnica de Lisboa (2009).
12. H. P. Tan, R. Diamant, W. K. G. Seah, M. Waldmeyer, A survey of techniques and challenges in underwater localization. *Ocean Eng.* **38**, 1663–1676 (2011).
13. F. Smith, “Understanding HPE in the VEMCO Positioning System (VPS)” (2013), , doi:VEMCO Document # Doc-005457-07.
14. T. M. Grothues, W. C. Davis, Sound pressure level weighting of the center of activity method to approximate sequential fish positions from acoustic telemetry. *Can. J. Fish. Aquat. Sci.* **70**, 1359–1371 (2013).
15. J. E. Edwards, J. Pratt, N. Tress, N. E. Hussey, Thinking deeper: Uncovering the mysteries of animal movement in the deep sea. *Deep Sea Res. Part I Oceanogr. Res. Pap.* **146**, 24–43 (2019).
16. M. R. Heupel, J. M. Semmens, A. J. Hobday, Automated acoustic tracking of aquatic animals: Scales, design and deployment of listening station arrays. *Mar. Freshw. Res.* **57**, 113 (2006).
17. J. K. Nielsen, G. Niezgoda, S. J. Taggart, S. J. Cooke, P. Anson, C. T. Hasler, K. C. Hanson, G. Carl, Mobile positioning of tagged aquatic animals using acoustic telemetry with a synthetic hydrophone array (SYNAPS: Synthetic Aperture Positioning System). *Am. Fish. Soc. Symp.* **76**, 233–250 (2012).
18. I. Masmitja, S. Gomariz, J. Del-Rio, B. Kieft, T. O’Reilly, P. J. Bouvet, J. Aguzzi, Optimal path shape for range-only underwater target localization using a Wave Glider. *Int. J. Rob. Res.* **37**, 1447–1462 (2018).
19. I. Masmitja, S. Gomariz, J. Del-Rio, B. Kieft, T. O’Reilly, P. J. Bouvet, J. Aguzzi, Range-Only Single-Beacon Tracking of Underwater Targets from an Autonomous Vehicle: From Theory to Practice. *IEEE Access*. **7**, 86946–86963 (2019).
20. K. L. Dodge, A. L. Kukulya, E. Burke, M. F. Baumgartner, TurtleCam: A “smart” autonomous underwater vehicle for investigating behaviors and habitats of sea turtles. *Front. Mar. Sci.* **5**, 1–10 (2018).
21. A. L. Kukulya, R. Stokey, R. Littlefield, F. Jaffre, E. M. H. Padilla, G. Skomal, 3D real-time tracking, following and imaging of white sharks with an Autonomous Underwater Vehicle. *MTS/IEEE Ocean. 2015 - Genova Discov. Sustain. Ocean Energy a New World*, 1–6 (2015).
22. N. Jepsen, C. Schreck, S. Clements, E. B. Thorstad, A brief discussion on the 2% tag/bodymass rule of thumb. *Aquat. Telem. Adv. Appl. Proc. Fifth Conf. Fish Telem. held Eur.*, 295 (2005).
23. C. M. Clark, C. Forney, E. Manii, D. Shinzaki, C. Gage, M. Farris, C. G. Lowe, M. Moline, Tracking and Following a Tagged Leopard Shark with an Autonomous Underwater Vehicle. *J. F. Robot.* **30**, 309–322 (2013).
24. C. F. White, Y. Lin, C. M. Clark, C. G. Lowe, Human vs robot: Comparing the viability and utility of autonomous underwater vehicles for the acoustic telemetry tracking of marine organisms. *J. Exp. Mar. Bio. Ecol.* **485**, 112–118 (2016).
25. R. D. Christ, R. L. Wernli, *The ROV Manual* (Elsevier, ed. 2nd, 2014).

26. T. M. Grothues, J. Dobarro, J. Ladd, A. Higgs, G. Niezgoda, D. Miller, Use of a multi-sensored AUV to telemeter tagged Atlantic sturgeon and map their spawning habitat in the Hudson River, USA. *2008 IEEE/OES Auton. Underw. Veh.*, 1–7 (2008).
27. T. M. Grothues, K. W. Able, J. H. Pravatiner, Winter flounder (Pseudopleuronectes americanus Walbaum) burial in estuaries: Acoustic telemetry triumph and tribulation. *J. Exp. Mar. Bio. Ecol.* **438**, 125–136 (2012).
28. M. J. Oliver, M. W. Breece, D. A. Fox, D. E. Haulsee, J. T. Kohut, J. Manderson, T. Savoy, Encogiendo el pajar: Utilización de un vehículo autónomo submarino en un observatorio oceánico integral para mapear el esturión del atlántico en el océano costero. *Fisheries*. **38**, 210–216 (2013).
29. J. H. Eiler, T. M. Grothues, J. A. Dobarro, M. M. Masuda, Comparing Autonomous Underwater Vehicle (AUV) and Vessel-based Tracking Performance for Locating Acoustically Tagged Fish. *Mar. Fish. Rev.* **75**, 27–42 (2014).
30. C. Lembke, S. Lowerre-Barbieri, D. Mann, J. C. Taylor, Using three acoustic technologies on underwater gliders to survey fish. *Mar. Technol. Soc. J.* **52**, 39–52 (2018).
31. D. Cote, J. M. Nicolas, F. Whoriskey, A. M. Cook, J. Broome, P. M. Regular, D. Baker, Characterizing snow crab (Chionoecetes opilio) movements in the sydney bight (Nova Scotia, Canada): A collaborative approach using multiscale acoustic telemetry. *Can. J. Fish. Aquat. Sci.* **76**, 334–346 (2019).
32. Y. Lin, J. Hsiung, R. Piersall, C. White, C. G. Lowe, C. M. Clark, A Multi-Autonomous Underwater Vehicle System for Autonomous Tracking of Marine Life. *J. F. Robot.* **34**, 757–774 (2017).
33. A. Ungfors, E. Bell, M. L. Johnson, D. Cowing, N. C. Dobson, R. Bublitz, J. Sandell, in *Advances in Marine Biology* (2013; https://linkinghub.elsevier.com/retrieve/pii/B9780124104662000078), vol. 64, pp. 247–314.
34. G. Z. Yang, J. Bellingham, P. E. Dupont, P. Fischer, L. Floridi, R. Full, N. Jacobstein, V. Kumar, M. McNutt, R. Merrifield, B. J. Nelson, B. Scassellati, M. Taddeo, R. Taylor, M. Veloso, Z. L. Wang, R. Wood, The grand challenges of science robotics. *Sci. Robot.* **3** (2018), doi:10.1126/scirobotics.aar7650.
35. H. C. So, Y. T. Chan, F. K. W. Chan, Closed-form formulae for time-difference-of-arrival estimation. *IEEE Trans. Signal Process.* **56**, 2614–2620 (2008).
36. Y. T. Chan, K. C. Ho, A simple and efficient estimator for hyperbolic location. *IEEE Trans. Signal Process.* **42**, 1905–1915 (1994).
37. H. Baktoft, K. Ø. Gjelland, F. Økland, U. H. Thygesen, Positioning of aquatic animals based on time-of-arrival and random walk models using YAPS (Yet Another Positioning Solver). *Sci. Rep.* **7**, 1–10 (2017).
38. A. N. Barkley, A. T. Fisk, K. J. Hedges, M. A. Treble, N. E. Hussey, Transient movements of a deep-water flatfish in coastal waters: Implications of inshore-offshore connectivity for fisheries management. *J. Appl. Ecol.* **55**, 1071–1081 (2018).
39. N. E. Hussey, K. J. Hedges, A. N. Barkley, M. A. Treble, I. Peklova, D. M. Webber, S. H. Ferguson, D. J. Yurkowski, S. T. Kessel, J. M. Bedard, A. T. Fisk, Movements of a deep-water fish: establishing marine fisheries management boundaries in coastal Arctic waters. *Ecol. Appl.* **27**, 687–704 (2017).
40. I. Jonsen, Joint estimation over multiple individuals improves behavioural state inference from animal movement data. *Sci. Rep.* **6**, 1–9 (2016).
41. V. Sbragaglia, F. Lamanna, A. M. Mat, G. Rotllant, S. Joly, V. Ketmaier, H. O. De La Iglesia, J. Aguzzi, Identification, characterization, and diel pattern of expression of canonical clock genes in Nephrops norvegicus (crustacea: Decapoda) eyestalk. *PLoS One*. **10**, 1–17 (2015).

42. I. D. Tuck, D. M. Parsons, B. W. Hartill, S. M. Chiswell, Scampi (Metanephrops challengeri) emergence patterns and catchability. *ICES J. Mar. Sci.* **72**, i199–i210 (2015).
43. J. G. Bellingham, Y. Zhang, J. E. Kerwin, J. Erikson, B. Hobson, B. Kieft, M. Godin, R. McEwen, T. Hoover, J. Paul, A. Hamilton, J. Franklin, A. Banka, Efficient propulsion for the Tethys long-range autonomous underwater vehicle. *2010 IEEE/OES Auton. Underw. Veh. AUV 2010*, 1–7 (2010).
44. E. Sollesnes, O. M. Brokstad, R. K. Boe, B. Vagen, A. Carella, A. Alcocer, A. P. Zolich, T. A. Johansen, Towards autonomous ocean observing systems using Miniature Underwater Gliders with UAV deployment and recovery capabilities. *AUV 2018 - 2018 IEEE/OES Auton. Underw. Veh. Work. Proc.*, 3–7 (2018).
45. J. Aguzzi, A. Mànuel, F. Condal, J. Guillén, M. Nogueras, J. del Rio, C. Costa, P. Menesatti, P. Puig, F. Sardà, D. Toma, A. Palanques, The new seafloor observatory (OBSEA) for remote and long-term coastal ecosystem monitoring. *Sensors*. **11**, 5850–5872 (2011).
46. J. Del-Rio, M. Nogueras, D. M. Toma, E. Martinez, C. Artero-Delgado, I. Bghiel, M. Martinez, J. Cadena, A. Garcia-Benadi, D. Sarria, J. Aguzzi, I. Masmitja, M. Carandell, J. Olive, S. Gomariz, P. Santamaria, A. Manuel Lazaro, Obsea: A Decadal Balance for a Cabled Observatory Deployment. *IEEE Access*. **8**, 33163–33177 (2020).
47. K. Doğançay, A. Hashemi-Sakhtsari, Target tracking by time difference of arrival using recursive smoothing. *Signal Processing*. **85**, 667–679 (2005).
48. B. Triggs, P. F. McLauchlan, R. I. Hartley, A. W. Fitzgibbon, in *International Workshop on Vision Algorithms* (Corfu, Greece, 2000; http://link.springer.com/10.1007/3-540-44480-7_21), pp. 298–372.
49. J. R. Magnus, J. R. Magnus, *Matrix Differential Calculus with Applications in Statistics and Econometrics* (Wiley, 2019), *Wiley Series in Probability and Statistics*.
50. S. Blackman, R. Popoli, *Design and Analysis of Modern Tracking Systems* (Artech House, 1999).
51. G. Huang, K. Zhou, N. Trawny, S. I. Roumeliotis, A bank of maximum A Posteriori (MAP) estimators for target tracking. *IEEE Trans. Robot.* **31**, 85–103 (2015).
52. C. H. Lee, Maximum a Posteriori Estimation for Multivariate Gaussian Mixture Observations of Markov Chains. *IEEE Trans. Speech Audio Process.* **2**, 291–298 (1994).
53. F. Meyer, O. Hlinka, H. Wymeersch, E. Riegler, F. Hlawatsch, Distributed Localization and Tracking of Mobile Networks Including Noncooperative Objects. *IEEE Trans. Signal Inf. Process. over Networks*. **2**, 57–71 (2016).
54. C. Forney, E. Manii, M. Farris, M. A. Moline, C. G. Lowe, C. M. Clark, Tracking of a tagged leopard shark with an AUV: Sensor calibration and state estimation. *Proc. - IEEE Int. Conf. Robot. Autom.*, 5315–5321 (2012).
55. O. Cappe, S. J. Godsill, E. Moulines, An overview of existing methods and recent advances in sequential Monte Carlo. *Proc. IEEE*. **95**, 899–924 (2007).
56. P. M. Djurić, J. H. Kotecha, J. Zhang, Y. Huang, T. Ghirmai, M. F. Bugallo, J. Míguez, Particle filtering. *IEEE Signal Process. Mag.* **20**, 19–38 (2003).
57. B. Jin, X. Xu, T. Zhang, Robust time-difference-of-arrival (Tdoa) localization using weighted least squares with cone tangent plane constraint. *Sensors (Switzerland)*. **18** (2018), doi:10.3390/s18030778.
58. J. Xavier, V. Barroso, *ICASSP, IEEE Int. Conf. Acoust. Speech Signal Process. - Proc.*, in press, doi:10.1109/ICASSP.2005.1416483.
59. K. Steven M., *Fundamentals of Statistical Signal Processing: Estimation Theory* (Prentice-Hall, Inc., 1993).
60. H. L. Van Trees, *Detection, Estimation, and Modulation Theory, Part I* (John Wiley and Sons, 2004).

61. C. Radhakrishna Rao, *Linear Statistical Inference and its Applications* (John Wiley & Sons, Inc., Hoboken, NJ, USA, 1973), *Wiley Series in Probability and Statistics*.
62. I. Masmitja, S. Gomariz, J. Del-Rio, B. Kieft, T. O'Reilly, J. Aguzzi, P.-J. Bouvet, C. Fannjiang, K. Katija, in *OCEANS 2019 - Marseille* (IEEE, 2019), pp. 1–10.
63. M. S. Arulampalam, S. Maskell, N. Gordon, T. Clapp, in *Bayesian Bounds for Parameter Estimation and Nonlinear Filtering/Tracking* (IEEE, 2009), vol. 50, pp. 723–737.
64. J. Zhang, D. Berleant, Envelopes around cumulative distribution functions from interval parameters of standard continuous distributions. *Annu. Conf. North Am. Fuzzy Inf. Process. Soc. - NAFIPS*. **2003-Janua**, 407–412 (2003).
65. G. K. Karagiannidis, A. S. Lioumpas, An improved approximation for the Gaussian Q-function. *IEEE Commun. Lett.* **11**, 644–646 (2007).
66. I. Masmitja, S. Gomariz, J. Del Rio, P. J. Bouvet, J. Aguzzi, Underwater multi-target tracking with particle filters. *2018 Ocean. - MTS/IEEE Kobe Techno-Oceans, Ocean. - Kobe 2018*, 1–5 (2018).
67. F. Arrichiello, G. Antonelli, A. Pedro Aguiar, A. Pascoal, An observability metric for underwater vehicle localization using range measurements. *Sensors (Switzerland)*. **13**, 16191–16215 (2013).
68. N. Crasta, D. Moreno-Salinas, B. Bayat, A. M. Pascoal, J. Aranda, Range-based underwater target localization using an autonomous surface vehicle: Observability analysis. *2018 IEEE/ION Position, Locat. Navig. Symp. PLANS 2018 - Proc.*, 487–496 (2018).
69. J. D. Quenzer, K. A. Morgansen, Observability based control in range-only underwater vehicle localization. *Proc. Am. Control Conf.*, 4702–4707 (2014).
70. E. W. Griffith, K. S. P. Kumar, On the observability of nonlinear systems: I. *J. Math. Anal. Appl.* **35**, 135–147 (1971).
71. I. Masmitja, S. Gomariz, J. Del Rio, B. Kieft, T. O'Reilly, Range-only underwater target localization: Path characterization. *Ocean. 2016 MTS/IEEE Monterey, OCE 2016*, 1–7 (2016).
72. D. Moreno-Salinas, A. Pascoal, J. Aranda, Optimal Sensor Placement for Acoustic Underwater Target Positioning with Range-Only Measurements. *IEEE J. Ocean. Eng.* **41**, 620–643 (2016).
73. N. Crasta, D. Moreno-Salinas, A. M. Pascoal, J. Aranda, Multiple autonomous surface vehicle motion planning for cooperative range-based underwater target localization. *Annu. Rev. Control*. **46**, 326–342 (2018).
74. B. Ha, G. Massion, "Coastal Profiling Float Depth Control" (Moss Landing, CA, 2018), (available at https://www.mbari.org/wp-content/uploads/2018/12/Ha.pdf).
75. G. B. Skomal, E. M. Hoyos-Padilla, A. Kukulya, R. Stokey, Subsurface observations of white shark Carcharodon carcharias predatory behaviour using an autonomous underwater vehicle. *J. Fish Biol.* **87**, 1293–1312 (2015).
76. D. Haulsee, M. Breece, D. Miller, B. Wetherbee, D. Fox, M. Oliver, Habitat selection of a coastal shark species estimated from an autonomous underwater vehicle. *Mar. Ecol. Prog. Ser.* **528**, 277–288 (2015).
77. D. R. Zemeckis, M. J. Dean, A. I. Deangelis, S. M. Van Parijs, W. S. Hoffman, M. F. Baumgartner, L. T. Hatch, S. X. Cadrin, C. H. McGuire, R. O'Driscoll, Identifying the distribution of Atlantic cod spawning using multiple fixed and glider-mounted acoustic technologies. *ICES J. Mar. Sci.* **76**, 1610–1625 (2019).
78. J. H. Eiler, T. M. Grothues, J. A. Dobarro, R. Shome, Tracking the movements of juvenile Chinook salmon using an autonomous underwater vehicle under payload control. *Appl. Sci.* **9** (2019), doi:10.3390/app9122516.
79. L. Zacher, "Tracking the Alaskan Red King Crab – Post 1-8, NOAA Alaska Fisheries Science Center" (2019).

80. J. S. Horne, E. O. Garton, S. M. Krone, J. S. Lewis, Analyzing animal movements using Brownian bridges. *Ecology*. **88**, 2354–2363 (2007).

Acknowledgments

Acknowledgments: We gratefully acknowledge the assistance and support of Larry Bird (MBARI) and the David and Lucile Packard Foundation. We would also like to thank Nixón Bahamón, José Antonio García, and Guiomar Rotllant for their help during the cruises. Ruth Durán helps us with the study area map. This work has been lead and carried out by members of the Tecnoterra associated unit of the Scientific Research Council through the Universitat Politècnica de Catalunya, the Jaume Almera Earth Sciences Institute and the Marine Science Institute (ICM-CSIC).

Funding: This work received financial support from different research projects of the Spanish *Ministerio de Economía y Competitividad* (RESNEP: CTM2017-82991-C2-1-R, RESBIO: TEC2017-87861-R, and SASES: RTI2018-095112-B-I00), of the *Generalitat de Catalunya* "*Sistemas de Adquisición Remota de datos y Tratamiento de la Información en el Medio Marino* (SARTI-MAR)" 2017 SGR 371, and NSF-IDBR (#145501 to K. Katija). J. Navarro was funded by the Spanish National Program Ramón y Cajal (RYC-2015-17809).

Author contributions: IM, JN, SG, JA, JDR and JBC conceived the presented idea, and planned the overall experiments. BK, TOR, CF and KK contributed to the design and implementation of the area-only target tracking research. IM developed the theory and performed the computations and performed the numerical simulations. PJB and AA verified the analytical methods. PP, MV, GV, NP and MC contributed to field tests preparation and the interpretation of the results. IM and JN wrote the manuscript with input from all authors. SG, JBC and KK supervised the project. All authors discussed the results and contributed to the final manuscript.

Competing interests: No competing financial interests exist.

Data and materials availability: GitHub github.com/imasmitja/TDOA_algorithms_SR

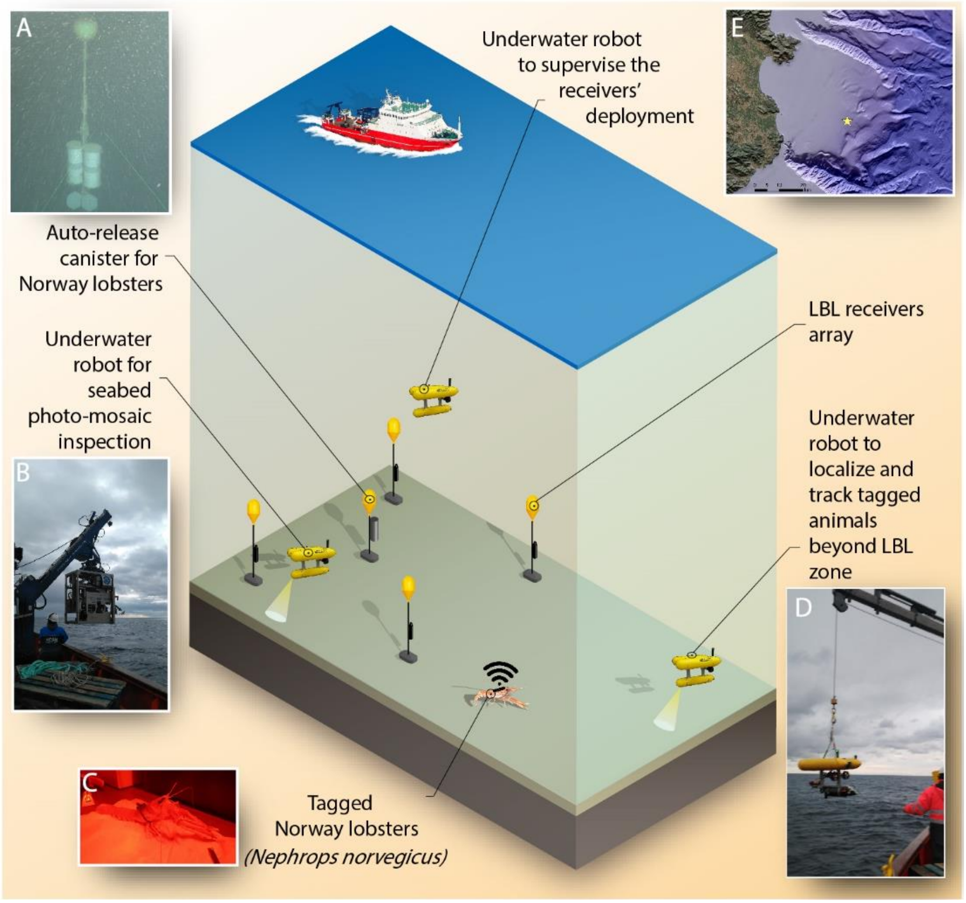

Fig. 1. Tracking deep water benthic marine animals. The strategy designed to track Norway lobsters (*Nephrops norvegicus*) is represented. Four receivers created an acoustic LBL localization system, where each one was in self-recording mode and was not accessed in real-time. The tags transmitted periodically an acoustic ping, which was recorded by the static receivers and the underwater vehicles, both systems were used to track the lobsters' movements. Moreover, different pictures detailing operations and systems are included: (**A**) the canister used to release the Norway lobsters, (**B**) the Super Mohawk II ROV, (**C**) a tagged Norway lobster showing the Vemco tag glued on its superior portion of the cephalothorax (manipulation of the lobsters occurred in red light to avoid eye damaging), and (**D**) the Girona500 AUV. The experiment was conducted in the northwest area of the Mediterranean Sea (**E**).

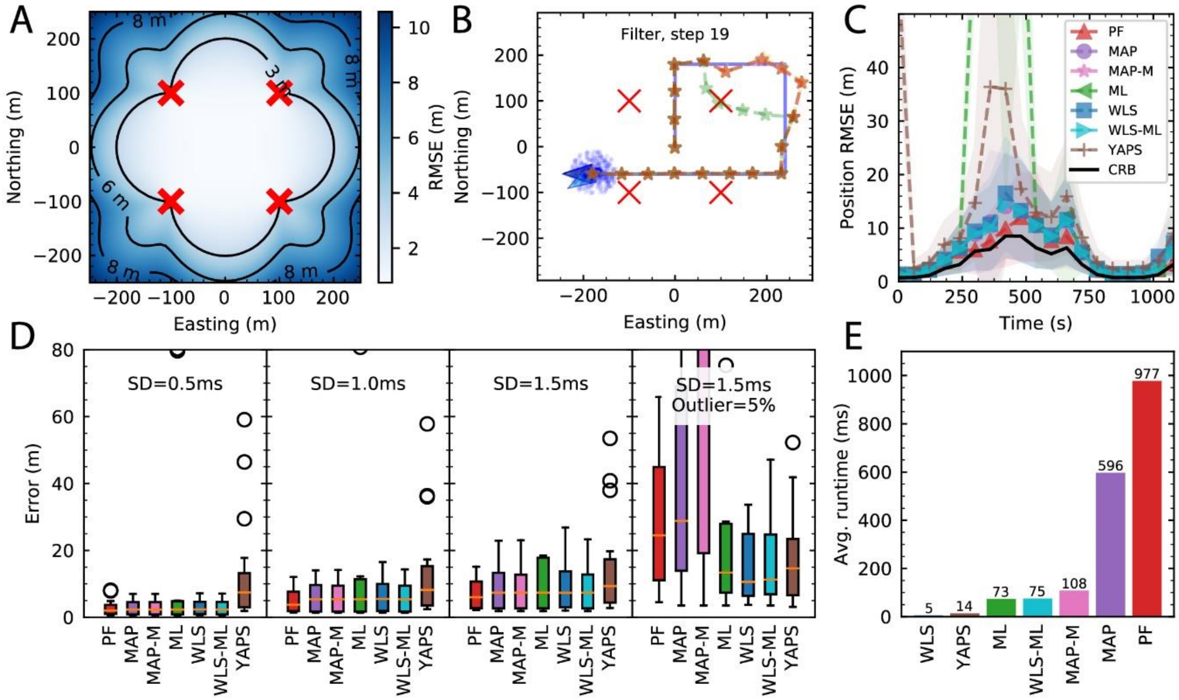

Fig. 2. TDOA algorithms performance. The CRB for TDOA target estimation (**A**), where the red crosses represent static receivers creating an acoustic LBL system. Target trajectory designed to compere the different TDOA algorithms' performance (**B**) are presented in relation to the particle filter (PF), the maximum a posteriori (MAP) estimation, the MAP marginalizing the latest measures (MAP-M), the maximum likelihood (ML) estimation, the weighted least squares (WLS), the WLS-ML, and the YAPS. The target estimation RMSE over the time (**C**), and the RMSE over 100 Monte Carlo iterations for all the algorithms (**D**), where different TDOA noise has been added ($\sigma = 0.5\ \text{ms},\ 1\ \text{ms},\ 1.5\ \text{ms}$), the plots show the median, and 5th and 95th percentiles. Finally, the average run-time required to compute one target position is shown (**E**).

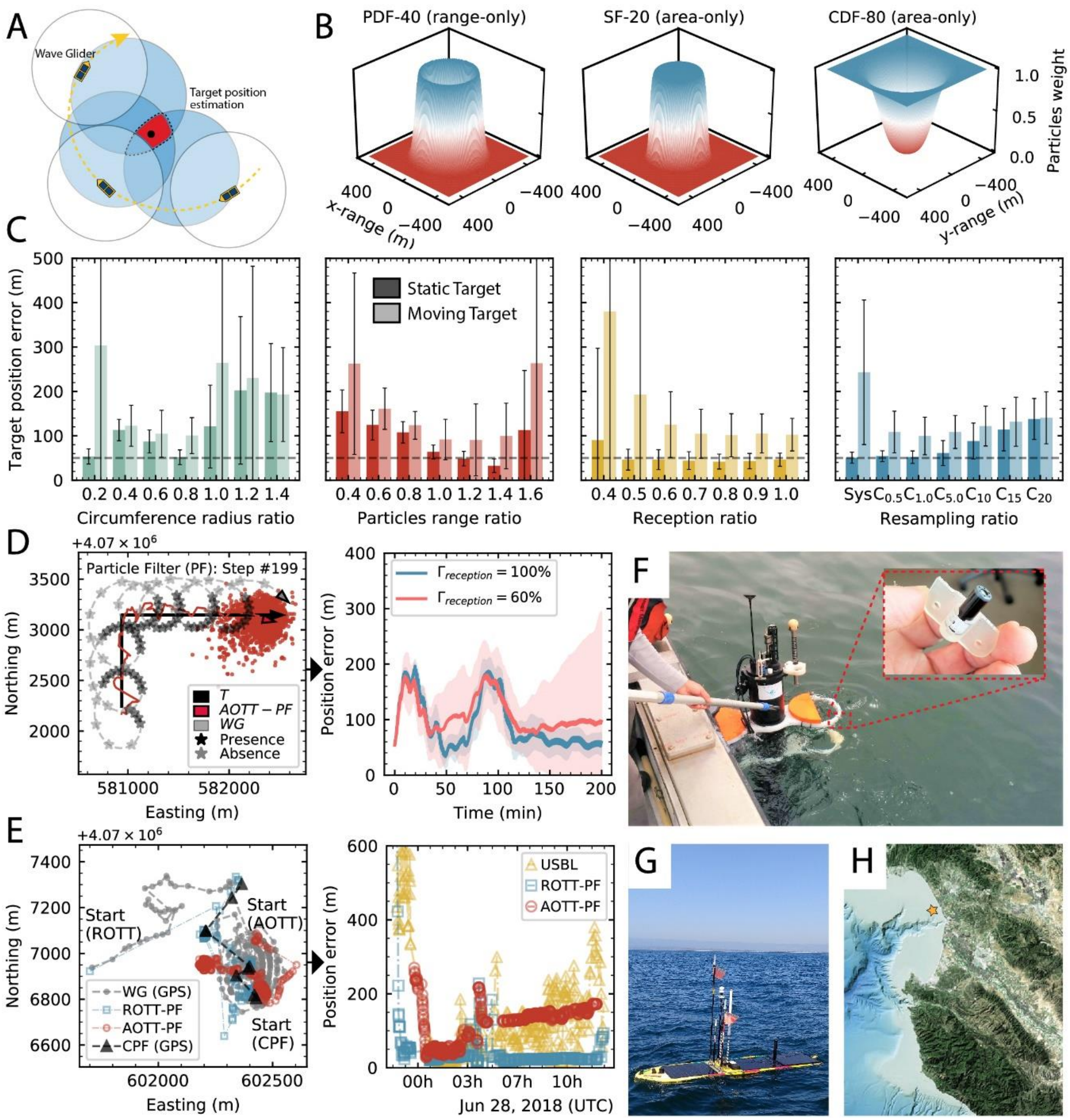

Fig. 3. AOTT method applied to the Monterey Bay test-site. AOTT method representation (**A**). Functions designed to weight the PF's particles (**B**). MC simulations to find the optimal value for different parameters (**C**), such as the circumference radius, the particles range, the reception, and the PF's resampling ratio, computed for static and moving targets. Simulations conducted to observe the AOTT's performance under different scenarios (**D**), where a reception ratio of 100% and 60% were used over 100 MC iterations. Results obtained during a field test (**E**), where a CPF (**F**) was used as a target and a Wave Glider (**G**) as an observer. Map of the study area in Monterey Bay, CA, USA (**H**).

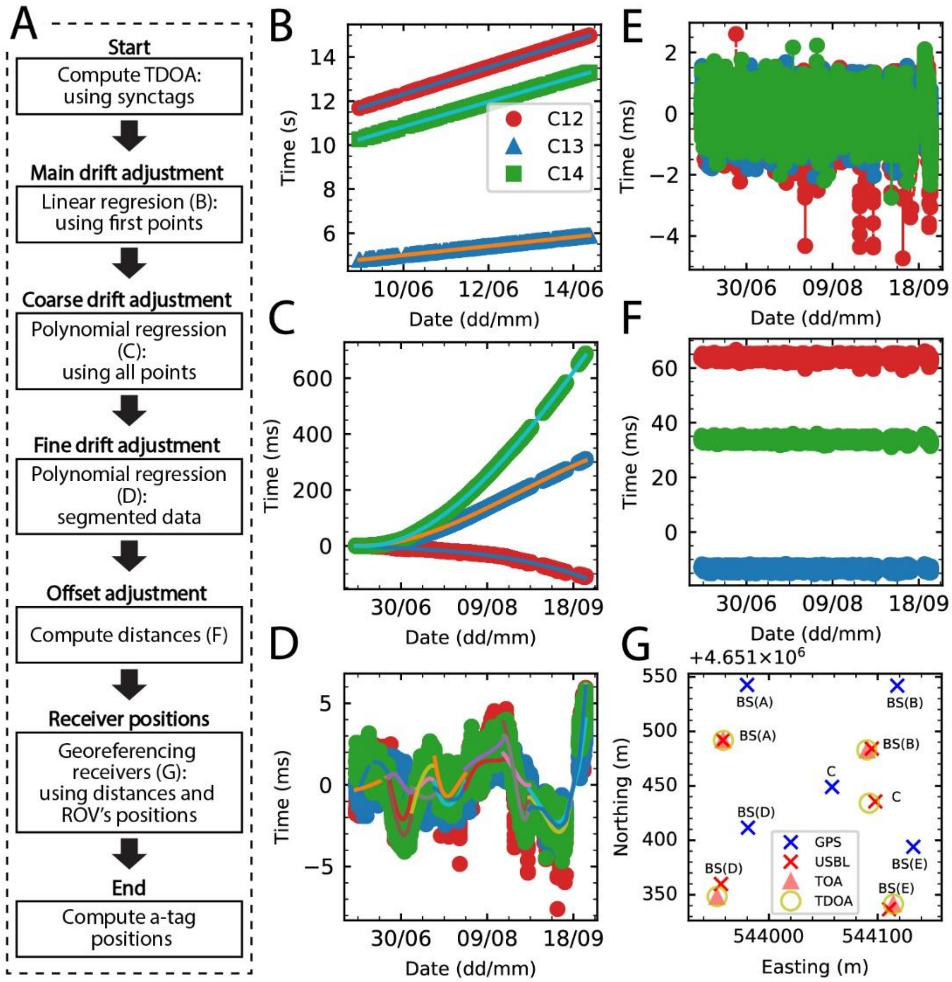

Fig. 4. Clock drift results during the Norway lobsters tracking. The synchronization process of the receivers can be observed in the flowchart (**A**). Then, the four-step process and the results obtained at each step are also presented as: the main drift at the beginning (**B**), the coarse drift after the first step (**C**), the fine drift (**D**), the TDOA error result and its outliers (**E**), and the final TDOA using a synchronization tag as a reference (**F**). C12, C13, and C14 denotes the difference between two receiver clock drifts. In addition, the positions of the moorings and the lobster canister in (**G**), where their initial position using the ship's GPS, the position obtained using the ROV's USBL, and the position computed acoustically are also pictured.

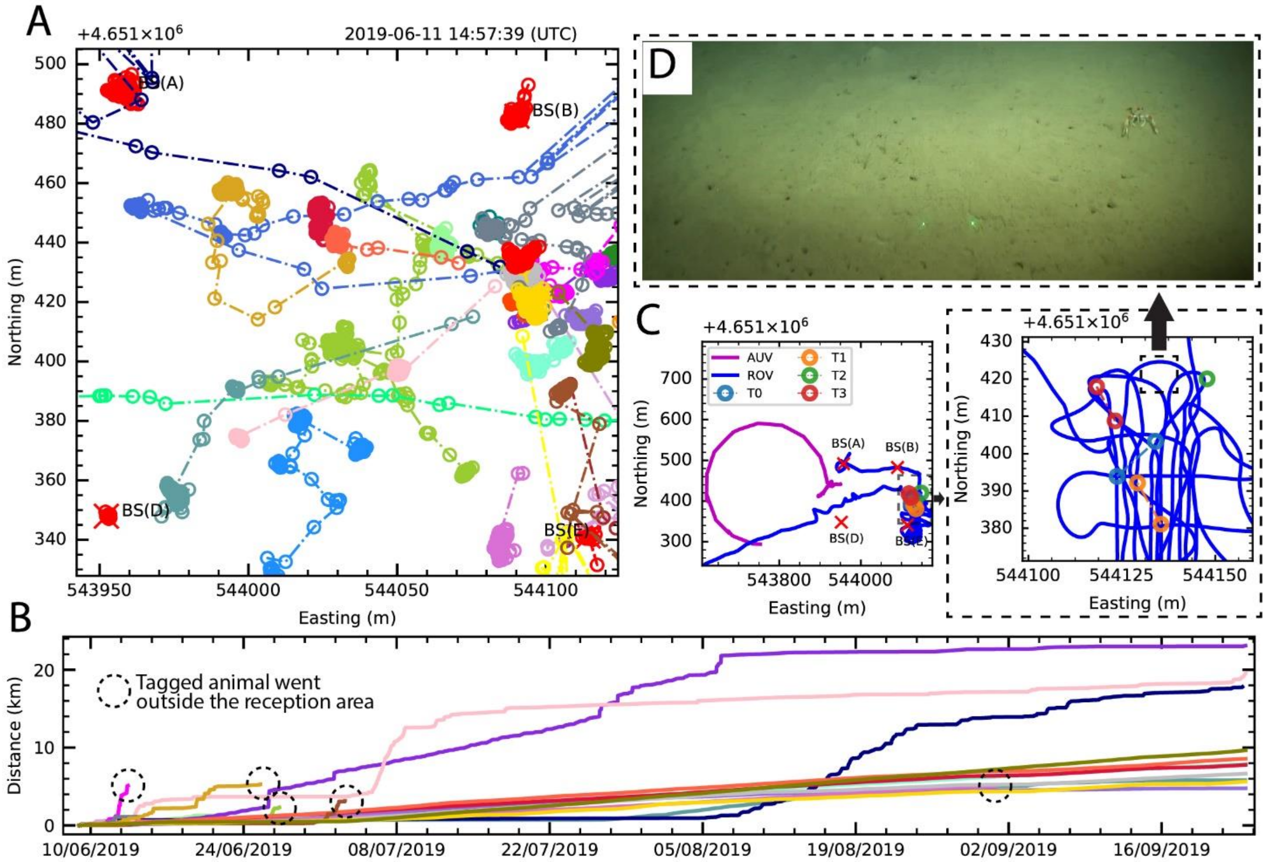

Fig. 5. Norway lobster tracking results. (**A**) The trajectories conducted by the tagged Norway lobsters during the moored experiment are represented, where the receivers are denoted as BS(X) and each tagged lobster has a different color. (**B**) The accumulative traveled distance covered by each tagged individual. (**C**) The different trajectories conducted by the underwater robots, in order to localize and track the Norway lobsters, where the receivers' localizations are represented by a red X and the detected tags denoted as T0-T3. Finally, an image obtained with the ROV HD camera (**D**), picturing the slope seabed with serval tunnel entrances and a wandering Norway lobster (15 cm distanced laser green-beams dots can also be observed).

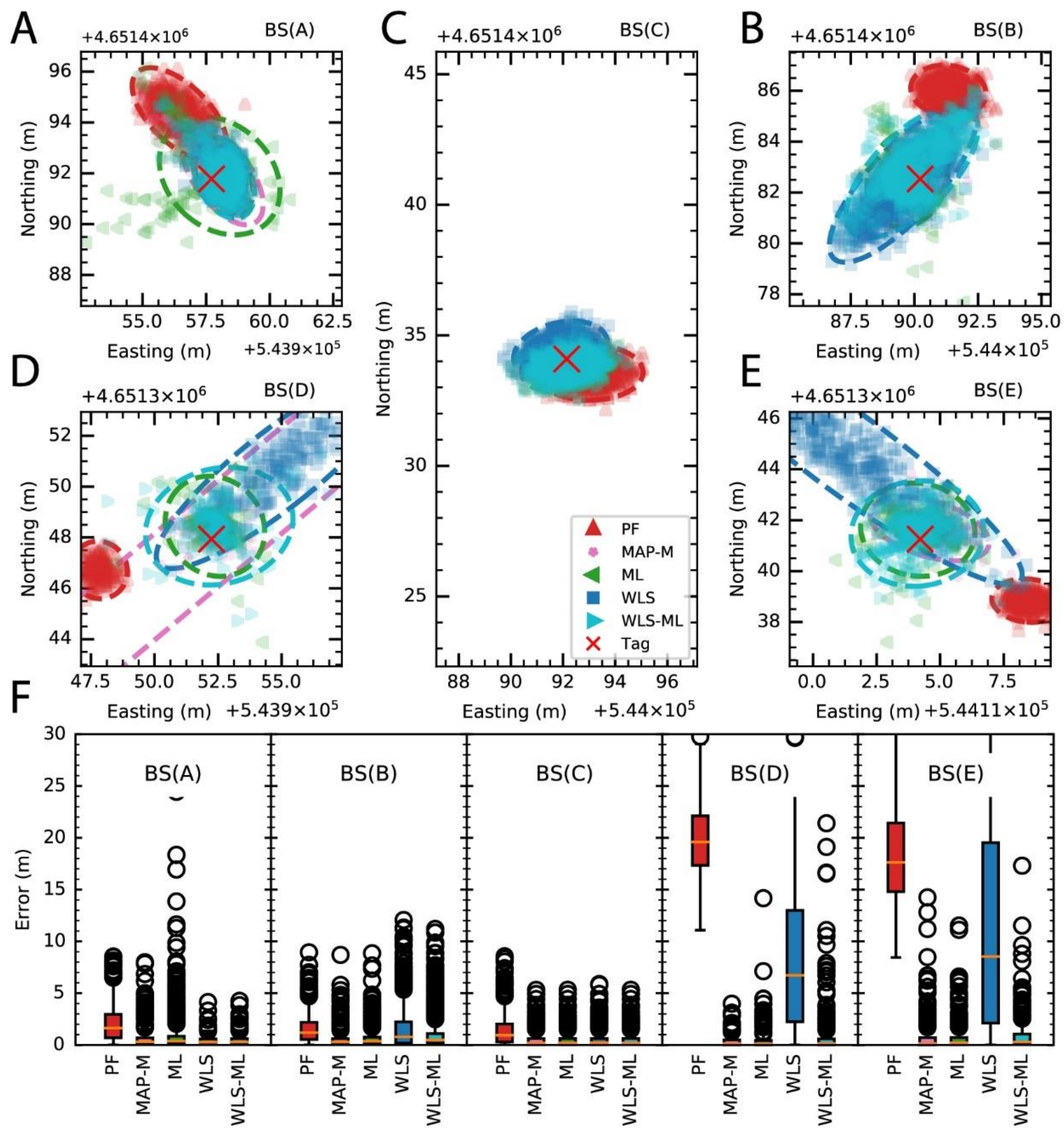

Fig. 6. Algorithms' performance during the Norway lobster experiment. Synchronization tag positions computed using different TDOA algorithms. These tags were attached on each mooring line alongside with a Vemco acoustic receiver (BS) (**A**, **B**, **D** and **E**). A last tag was mounted on the lobster canister, which was deployed on the center of the experiment (**C**). The error covariance matrix with a confidence interval of 98% is also presented. This information is presented as error bars in (**F**). The plots show the median, and 5th and 95th percentiles.

Table 1. Mooring lines positioning error. Position of the moorings obtained using the ROV and the TOA signals (Position 1) compared with the positions computed using the WLS-ML algorithm (Position 2), and the associated error.

Moorings	Position 1		Position 2		Error (m)	SD (m)
	x (m)	y (m)	x (m)	y (m)		
BS(A)	543957.71	4651491.78	543958.24	4651491.60	0.74	0.55
BS(B)	544090.23	4651482.54	544089.80	4651482.68	0.68	0.40
BS(C)	544092.14	4651434.09	544092.10	4651433.95	1.29	1.05
BS(D)	543952.24	4651347.94	543952.56	4651348.23	0.51	0.29
BS(E)	544114.21	4651341.26	544114.03	4651341.52	0.48	0.27

Table 2. Target tracking experiments using underwater robots. Different campaigns conducted to localize and follow a marine tagged animal using both fixed receivers and/or underwater vehicles (aka dynamic transponders)

								Static transponders				Dynamic transponders					
Year	**Location**	**Species**	**#**	**Tag type**	**Tag size (mm)**	**Time**	**Depth (m)**	**Method**	**Acoustic range (m)**	**Algorithm**	**Error (m)**	**Method**	**Acoustic range (m)**	**Algorithm**	**Error (m)**	**Vehicle**	**Ref.**
2008	Hudson R.	*A.O. oxyrinchus*	2	MAP32 1s	32x101	2 d	~18	-	-	-	-	TDOA	NR	SYNAPS‡	25	REMUS-100 AUV	(*26*)
2013	Navesink R.	*P. americanus*	39	MA-TP11 18	○	51d	< 8	LBL	NR	TDOA* / SPLWCA	~2	Presence	~890	-	-	REMUS-100 AUV	(*14*, *27*)
2013	Caribbean S.	*M. undulatus*	1	MA-TP11 18	○	7 h	10	-	-	-	-	SPL	NR	SPLWCA	NR	REMUS-100 AUV	(*14*)
2013	NW Atlantic	*A.O. oxyrinchus*	4	V16 69kHz	16x54	1095 d	~90	Gate F.§	~800	-	-	Presence	NR	-	-	Slocum G2 Glider	(*28*)
2014	N Pacific	*A. fimbria* and *P.camtschaticus*	41	MA-TP16-33	62x16	61 d	< 585	NR	NR	NR	NR	Presence	~500	-	-	REMUS 100 AUV	(*29*)
2015	NE Pacific	*C. carcharias*	6	Transp.†	76x380	12 h	93-130	-	-	-	-	USBL	NR	NR	NR	REMUS 100 AUV	(*21*, *75*)
2015	NW Atlantic	*C. taurus*	292	V16 69kHz	16x54	12 d	<25	Gate F.§	~800	-	-	Presence	250	-	-	Slocum G2 Glider	(*76*)
2016	NE Pacific	*T. semifasciata*	1	MM-M-16-50	16x80	3 d	< 100	-	-	-	-	Bearing	NR	PF	80	Iver2 AUV	(*24*)
2017	NE Pacific	*T. semifasciata*	3	Smart Tag††	200x127	3 d	< 10	-	-	-	-	Bearing	NR	PF	~10	Iver2 AUV	(*32*)
2018	NE Pacific	*D. coriacea*	9	Transp.†	76x380	36 h	0-20	-	-	-	-	USBL	NR	NR	NR	REMUS 100 AUV	(*20*)
2018	G. Mexico	*E. morio* and *L. campechanus*	61	V13P L	13x36	365 d	30-60	Presence	NR	-	NR	Presence	NR	-	NR	Slocum G1 Glider	(*30*)
2019	NW Atlantic	*C. opilio*	164	V13 and V9	13x36	720 d	~116	LBL	NR	VPS**	NR	Presence	~500	DWA‡‡	NR	Wave Glider	(*31*)
2019	NW Atlantic	*G. morhua*	317	V16-6H	16x54	720 d	< 50	Fisheries F.§	~1000	BBMM***	NR	Presence	~1000	BBMM***	NR	Slocum G2 Glider	(*77*)
2019	G. Alaska	*O. tshawytscha*	20	MM-M-8-S0	8.5x43	7 d	30-100	-	-	-	-	TDOA	~500	SYNAPS‡	NR	REMUS 100 AUV	(*78*)
2019	Bering S.	*P. camtschaticus*	150	Vemco	NR	365 d	<100	-	-	-	-	NR	NR	NR	NR	Saildrone ASV	(*79*)

¶Species names: *Acipenser oxyrinchus oxyrinchus, Pseudopleuronectes americanus, Micropogonias undulatus, Anoplopoma fimbria, Paralithodes camtschaticus, Carcharodon carcharias, Carcharias taurus, Triakis semifasciata, Dermochelys coriacea, Epinephelus morio, Lutjanus campechanus, Chionoecetes opilio, Gadus morhua, Oncorhynchus tshawytscha, and Paralithodes camtschaticus*

NR = Information not reported
○= Information not found
- = Information not applicable
†Designed by WHOI
††The SmartTag package consist of an IMU, a Lotek MM-M-16-50-PM acoustic tag, a VHF transmitter and a video logger system
§ See M. R. Heupel et al. (*16*)
* Using ALPS: Asynchronous Logging Positioning System software (Lotek Wireless, Inc.)
**VPS: Vemco Positioning System array
***BBMM: Brownian Bridge Movement Model (*80*)
‡SYNAPS: synthetic hydrophone array, proprietary software from Lotek
‡‡DWA = Daily Weighted Average

SUPPLEMENTARY MATERIALS

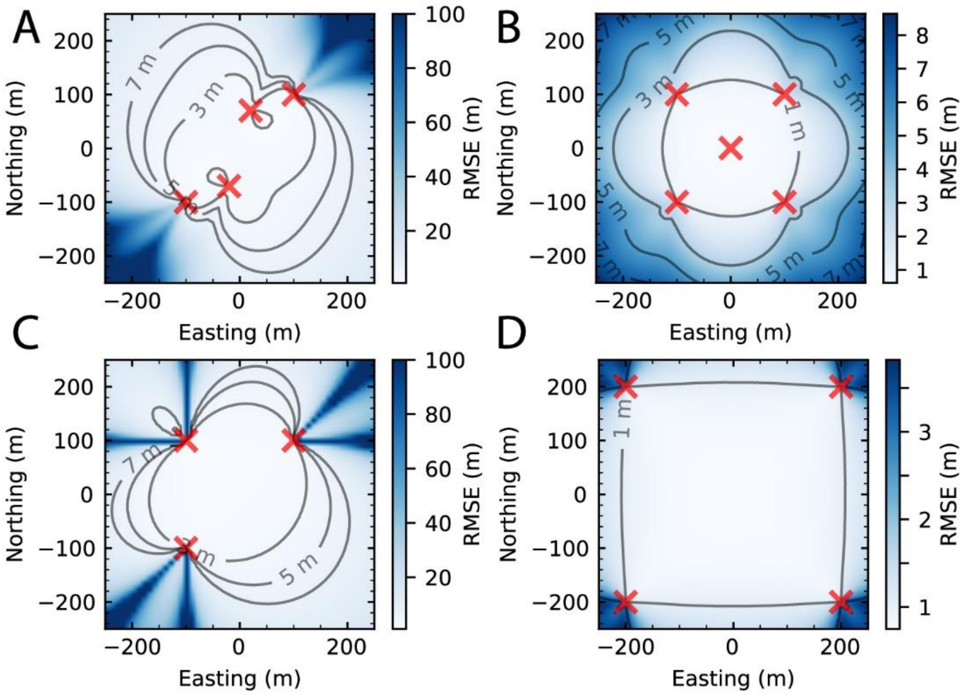

Fig. S1. Algorithms’ performance vs receivers’ position. The CRB for TDOA target estimation using different receivers’ configuration (red crosses). (**A**) four receivers using a non-square shape. Using five receivers the error is reduced (**B**), whereas using only three receivers the error clearly augments (**C**). If the separation between receivers is augmented (i.e. we have a greater baseline distance), so does the accuracy (**D**).

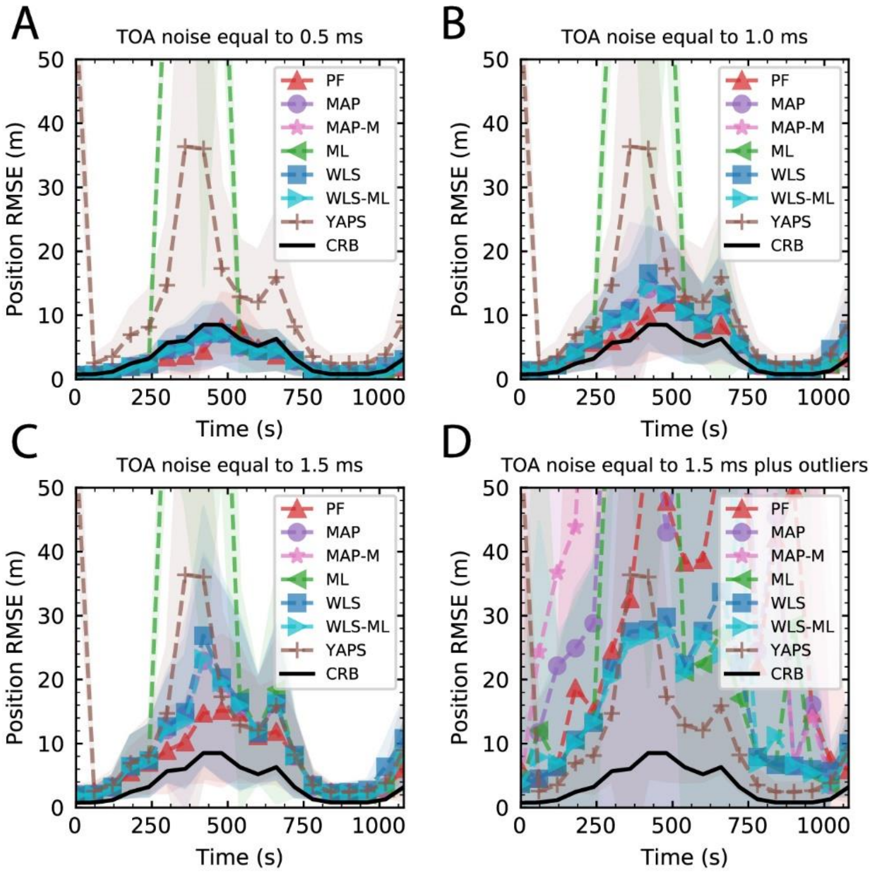

Fig. S2. TDOA algorithms performance over the time. The RMSE evolution over the time for different algorithms and compered with CRB. (**A**) using a Gaussian noise of 0.5 ms added at each TOA measurement, (**B**) using a Gaussian noise of 1.0 ms, (**C**) using a Gaussian noise of 1.5 ms, and (**D**) using a Gaussian noise of 1.5 ms plus a random outlier (i.e. multiplying by 4 the TOA measured).

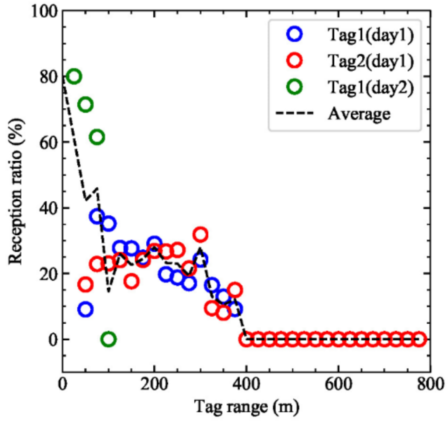

Fig. S3. Reception ratio. Reception ratio versus distance between devices. Results obtained during field trials in Monterey Bay, California, between a Wave Glider and an acoustic tag (V7P-69 kHz).

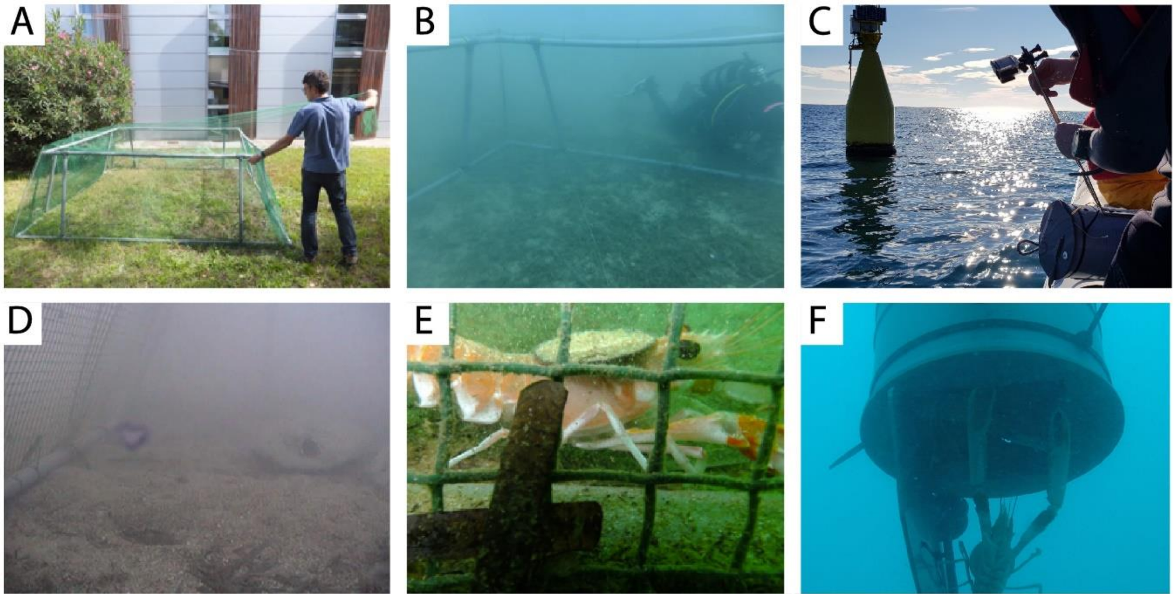

Fig. S4. Fieldwork methods evaluation at the OBSEA platform. The OBSEA (www.obsea.es) is an underwater cabled observatory located at 20 m depth in the “Coll Mira el Peix” Marine Protected (EU Natura 2000 network) area. (**A**) The cage was built at the Universitat Politècnica de Catalunya facilities. (**B**) the cage installation by divers at the cabled observatory, in front of the video camera. (**C**) Testing the automatic release canister to release the Norway lobsters. (**D**) Different artificial burrows, made by PVC pipes buried in concrete, were also installed inside the cage. (**E**) a Norway lobster inside the cage (with an attached visual tag mimicking the Vemco emitter and also used to facilitate the remote visual inspection *via* the camera). And (**F**) one of the animals being released by the canister.

Table S1. Algorithms' performance during the Norway lobster experiment. Error and standard deviation of each Vemco acoustic receiver (BS) and the lobster canister (denoted as BS(C)), and their synchronization tag associated, using different TDOA algorithms.

	BS(A)		BS(B)		BS(C)		BS(D)		BS(E)	
Algorithms	**error (m)**	**SD (m)**	**error (m)**	**SD (m)**	**error (m)**	**SD (m)**	**error (m)**	**SD (m)**	**error (m)**	**SD (m)**
PF	3.20	0.46	3.85	0.20	0.48	0.29	5.36	0.17	10.28	0.16
MAP-M	0.06	0.43	0.06	0.47	0.02	0.25	-	-	0.15	0.40
ML	0.04	0.75	0.01	0.41	0.02	0.25	0.07	0.52	0.04	0.56
WLS	0.03	0.25	0.12	1.22	0.08	0.28	7.07	2.52	9.02	4.67
WLS-ML	0.03	0.27	0.09	0.92	0.02	0.25	0.15	0.91	0.02	0.74

Movie S1. Simulation of target tracking using TDOA. One of the simulations conducted to observe the performance of different algorithms for target tracking using TDOA signals.

Movie S2. Simulation of target tracking using AOTT. One of the simulations conducted to observe the performance of tagged target tracking using the AOTT algorithm.

Movie S3. Norway lobster movements. Trajectory conducted by the 33 Norway lobsters tagged during the RESNEP campaign, first three days.

Movie S4. Seabed images. Images of the seabed obtained inside the area of the Norway lobster experiment by the ROV.